PURDUE UNIVERSITY

Team Shadow Drag

2008 AIAA Cessna/Raytheon Student Design/Build/Fly Competition

LOCKHEED MARTIN

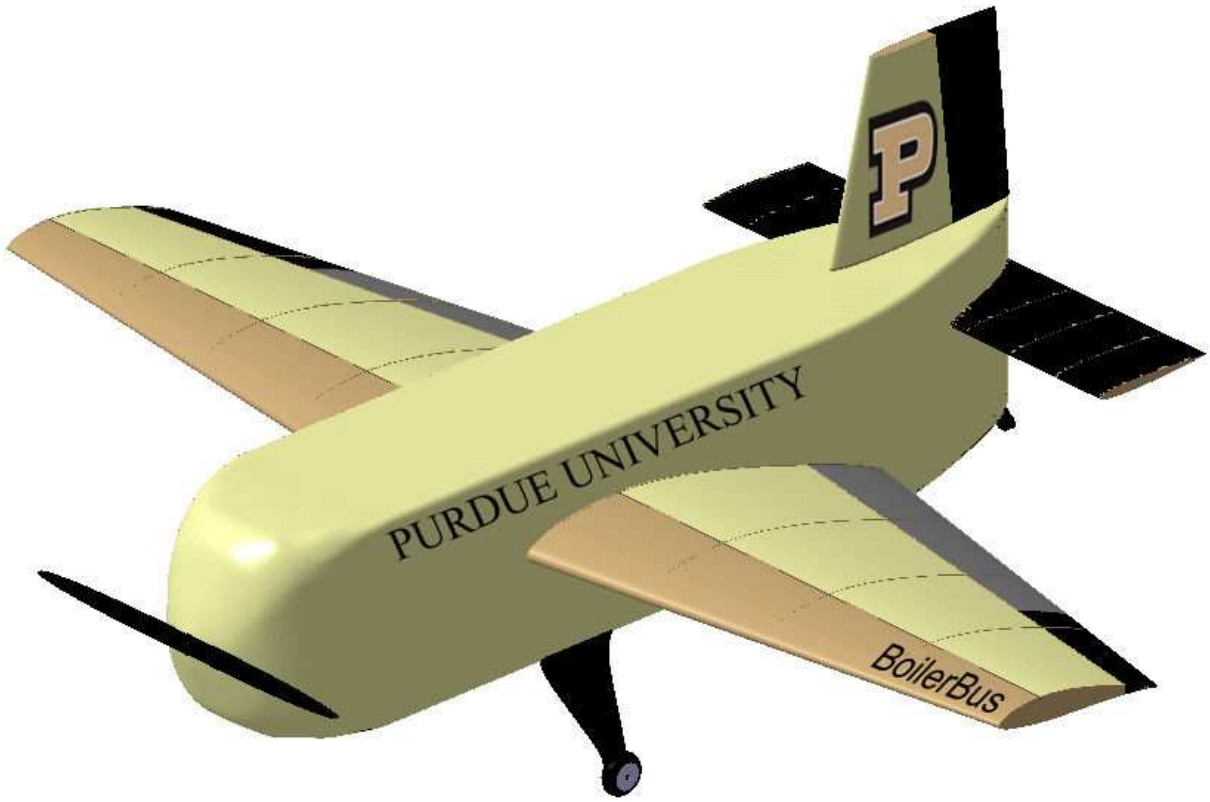

TABLE OF CONTENTS

1 EXECUTIVE SUMMARY

This report describes the design, manufacturing, and testing techniques used for the development of Purdue University's entry to the 2007-2008 AIAA Student Design/Build/Fly Competition. Competition rules constrain the aircraft geometry to a 4' x 5' area and require take-off within 75'. The missions include a fixed flight profile with and without a nominal 7 lbf payload, with timed loading of payloads. A spiral design approach was used to systematically design and optimize an aircraft to yield the highest total score. The total score is a combination of the written report score, total flight score, and rated aircraft cost (RAC).

The first design spiral was accomplished in four stages: conceptual design, preliminary design, manufacturing, and testing. During the conceptual design, the competition rules and requirements were analyzed to identify and weigh Figures of Merit (FOM). Selection matrices based on the FOM were used to narrow aircraft selection to three types: conventional, blended wing body, and joined wing. The joined wing aircraft was eliminated due to its high risk and time constraints. Preliminary design focused on refining the two remaining aircraft on the basis of simulated mission performance and scores. The two aircraft were then built and wind tunnel tested. The conventional aircraft, nicknamed BoilerBus1, was also flight tested. The actual construction and testing of the aircraft provided valuable data that validated theoretical models and led to the final down-selection of a conventional aircraft configuration.

The second design spiral consisted of three stages: detailed design, manufacturing, and testing. The optimization of the conventional aircraft was the focus in detailed design. Wing/fuselage geometry and empennage sizing analysis were conducted first to refine the aircraft's stability and aerodynamic performance. Propeller testing provided data for propulsion systems analysis, and selection of the optimal battery, motor, and propeller combination. Aerodynamic and structural computational models of the entire aircraft were analyzed and validated with wind tunnel and flight tests. Figure 1.1 illustrates the design approach of the aircraft via the design spiral. The final aircraft configuration is shown in Figure 1.2.

The conventional aircraft is a well-established, stable design that is simple to manufacture. The design is also a proven platform for the efficiency and heavy lifting capability requirements of the flight missions. The use of flaps helps meet the take-off distance requirement while minimizing propulsion system size. This is also augmented by the take-off configuration dictated by the tail dragger landing gear. The mid-wing provides easy access to the top of the fuselage for fast loading while providing required stability. The payload bay is bilaterally symmetric about the nominal center of gravity, allowing the CG envelope to remain within 0.25" for all payload combinations. The wing taper ratio of 0.45 approximates elliptical load distribution, minimizing induced drag and reducing the bending moment at the root, minimizing structural requirements. Finally, a stabilator was used to minimize surface area and decrease drag and weight.

The final design had a predicted maximum lift to drag ratio of 6.3 and Mission 2 RAC of 1.58. The RAC includes a system weight of 3.65 lbf and payload mission battery weight of 0.54 lbf. To maximize the Mission 1 score, the aircraft would fly 1 lap, requiring a battery weight of 0.12 lbf.

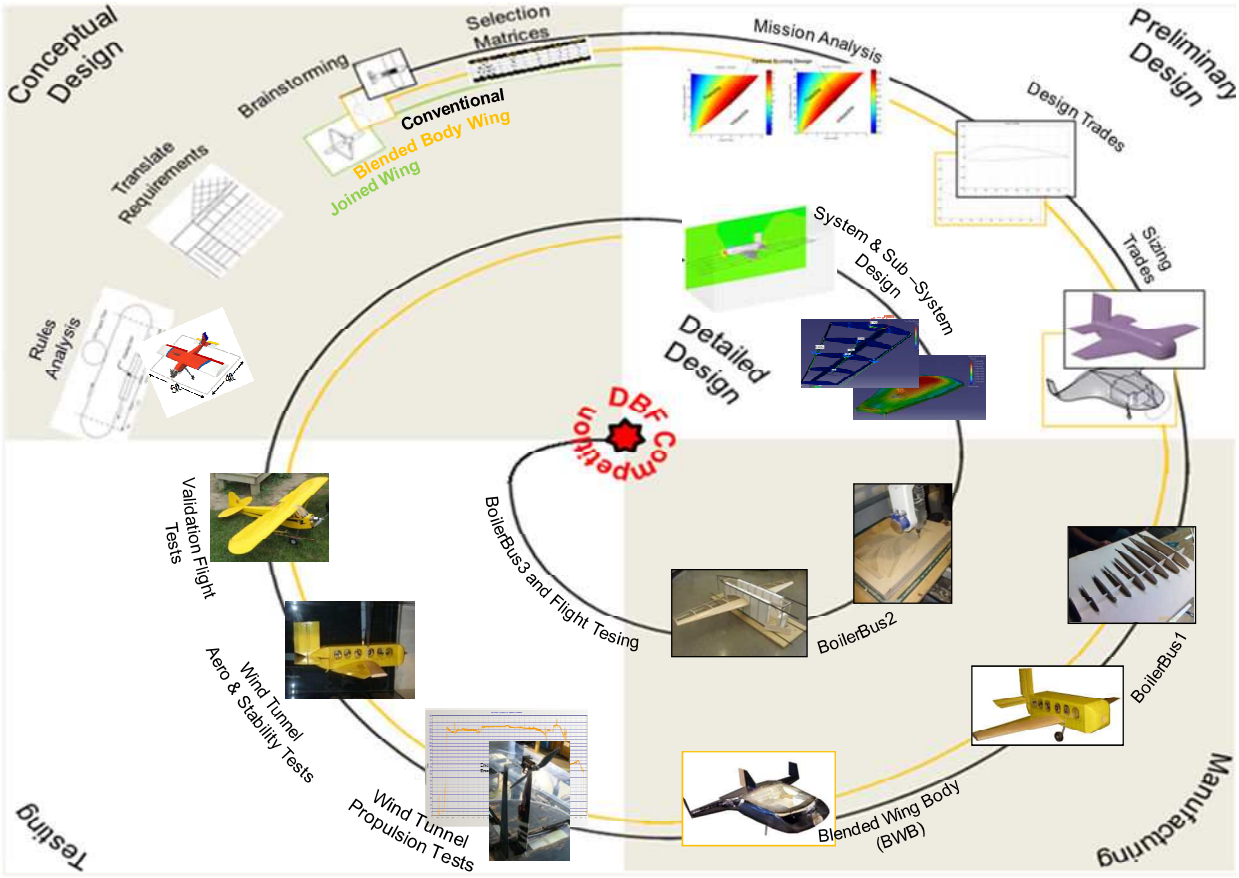

Figure 1.1: Design Spiral

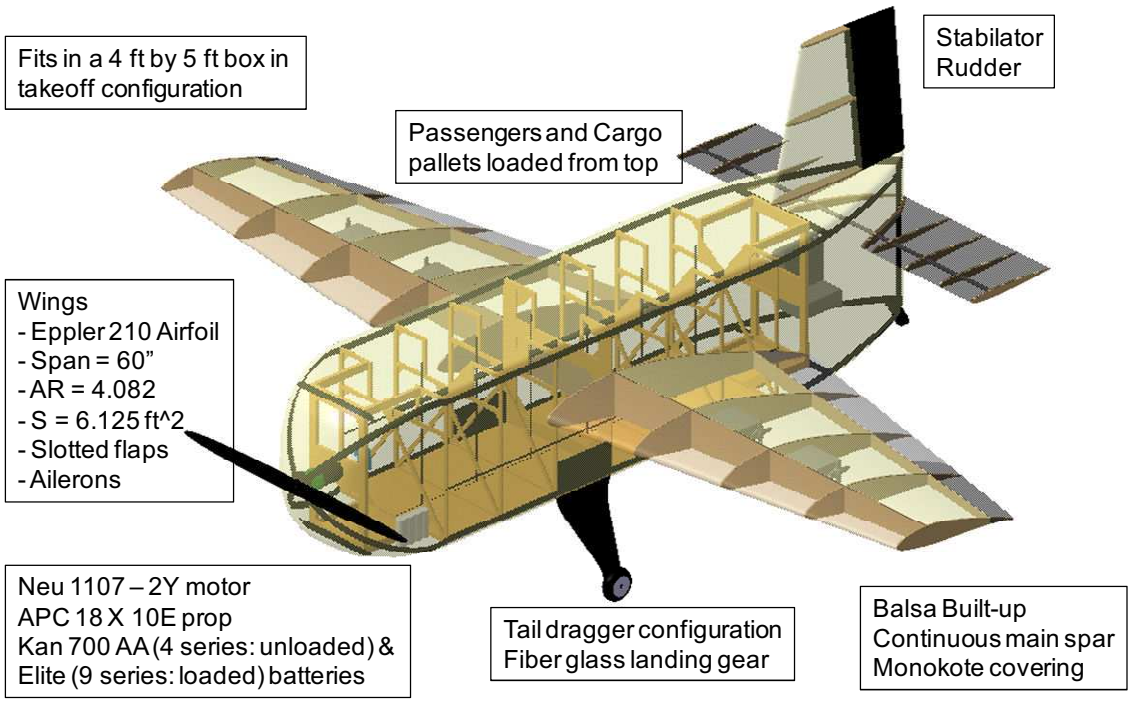

Figure 1.2: Aircraft Walk Around

2 MANAGEMENT SUMMARY

2.1 Team Organization and Assignment Areas

The Shadow Drag team was recruited to include several students of diverse class standings. Members were required to independently analyze the rules and scoring factors and brainstorm aircraft configurations. During preliminary aircraft sizing, members were separated into sub-teams to promote innovative and competitive design. After the aircraft configuration down-selection, team members were assigned to sub-teams in the areas of aerodynamics, structures, propulsion, stability, manufacturing, and testing. Each sub-team was assigned a team leader to create a management hierarchy for efficient team management. Figure 2.1 lists the team members and their primary areas of responsibility.

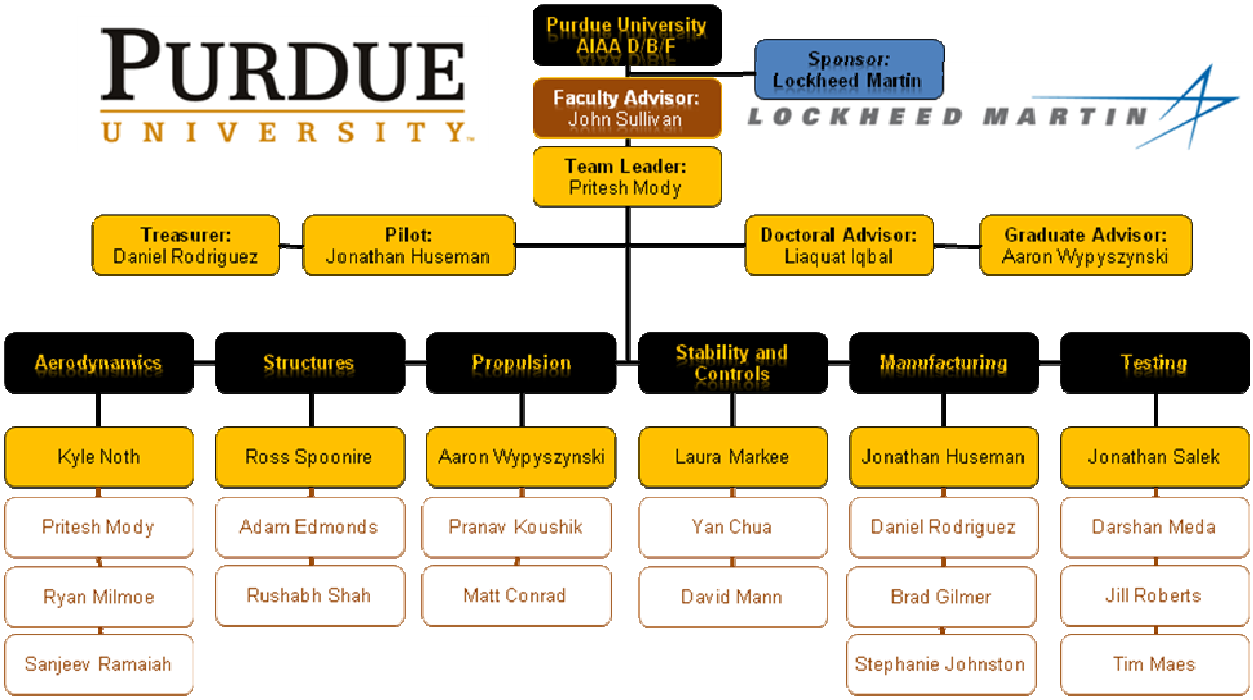

Figure 2.1: Team Organization Chart

2.2 Project Milestone Chart

The successful design, construction, and testing of an aircraft is a complex task that requires a well managed team. The first step, therefore, was to organize a team and develop a balanced project schedule with routine design reviews. The master project schedule with planned and actual schedules and milestones is provided in Figure 2.2.

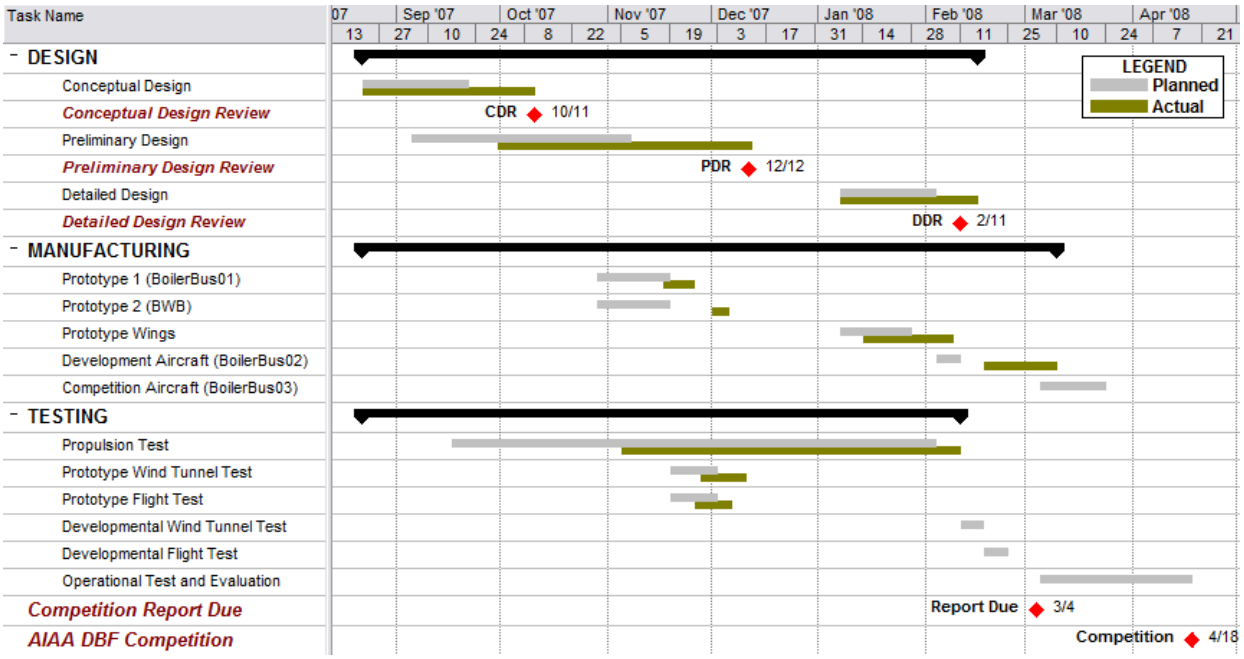

Figure 2.2: Master Project Schedule

3 CONCEPTUAL DESIGN

The goals of conceptual design include the analysis of mission rules and their translation into design requirements using Quality Function Deployment. Brainstorming identified concepts to meet those requirements, and these concepts were compared using Figures of Merit. The end result of the process, as shown in Figure 3.1, was the identification of configurations for quantitative analysis in preliminary design.

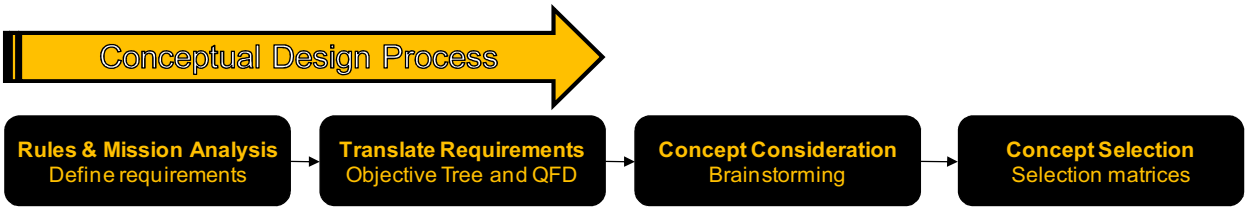

Figure 3.1: Conceptual Design Process

3.1 Requirements

Aircraft and mission requirements are stipulated in the contest rules specific for the 2008 AIAA Design/Build/Fly competition. Strict adherence is required for competition eligibility.

3.1.1 Aircraft

The aircraft may be any configuration except rotary wing or lighter-than-air. The regulations also specified that it must be driven by commercially available propellers, electric-powered with one or more unmodified over-the-counter brush or brushless electric motor(s), and use NiCad or NiMH batteries. Motors and

batteries will be limited to a maximum of 40 Amp current draw and a maximum battery weight of 4 lbf. The entire aircraft must fit in a 4' x 5' rectangle in take-off configuration with no parts crossing outside of this boundary as shown in Figure 3.2.

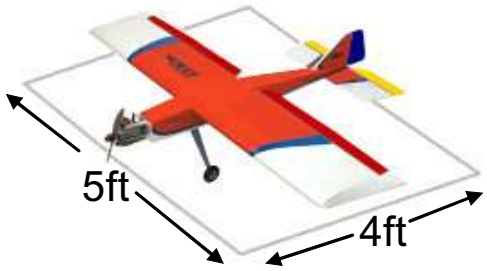

Figure 3.2: Aircraft Sizing Requirement

3.1.2 Payloads

The payloads consist of ½ liter plastic bottles to simulate passengers and half-size clay bricks to simulate cargo pallets. The bottles weigh approximately ½ lbf each, have a diameter of 2.5", and a height of 8.5" with 4" diameter or 4" x 4" square collars. The bricks will each weigh approximately 1.8 lbf and have a nominal size of 4" x 4" x 2.7" Several different payload combinations are possible, with total payload weight ranging from 6.8 to 7.2 lbf. Payloads will be assigned randomly at the competition. The payloads are shown in Figure 3.3.

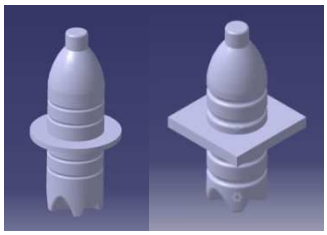

	Bottles	Bricks	Weight (lbf)
1	14	0	7.0
2	0	4	7.2
3	10	1	6.8
4	7	2	7.1
5	3	3	6.9

Figure 3.3: Payloads and Payload Combinations

3.1.3 Mission Profiles

Each team is required to complete three missions in a maximum of five total attempts. The course layout defining one lap is shown in Figure 3.4. Successful completion requires take-off in 75'. The upwind leg consists of 500' segment, followed by a crosswind 180° turn, 1000' downwind leg which includes a 360° turn segment, 180° base turn, a 500' final leg segment, and a successful landing.

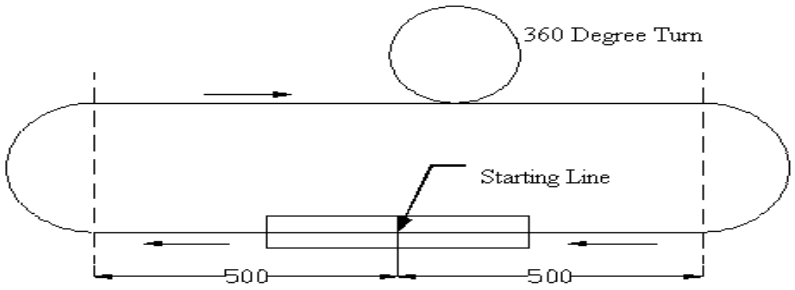

Figure 3.4: Course Layout

Delivery Flight (Mission 1): The aircraft will have no payload for this mission. Teams will attempt to complete the greatest number of complete laps, subject to battery weight, within a 5 minute time period. The delivery flight must be successfully completed before teams can attempt the payload flight missions.

Payload Flight (Mission 2): The aircraft will fly two different payload missions, each consisting of a different payload combination. The aircraft must fly two laps following a timed loading of the payloads.

3.1.4 Scoring

All flight scores are normalized across all successful aircraft flying that mission.

- Delivery Mission Score (50 pts max) = Number of completed laps / Battery weight for Mission 1
- Payload Mission Score (50 pts max/flight) = 1 / (Loading Time * RAC)
  where Rated Aircraft Cost (RAC) = System weight * Battery weight for Mission 2
- Total Flight Score (150 pts max) = Delivery Mission Score + Payload Mission Score 1 + Payload Mission Score 2
- Total Score (15000 pts max) = Written Report Score (100 pts max) *Total Flight Score (150 pts max)

3.2 Mission Design

Structured design methods were applied during the conceptual design phase. The methods employed include an Objective Tree, Quality Function Deployment (QFD), brainstorming, and organization of concepts through an affinity diagram. Concept selection was made through decision matrices based on FOM.

3.2.1 Objectives Tree

An Objectives Tree [1], as shown in Figure 3.5, was created as a requirement review process. As the tree works down, the points become more specific and answer the question of how the above solution will be achieved. Conversely, working up the tree answers the question of why the lower points are desired. The most specific design solutions established were high propulsive efficiency, high wing loading, low stall velocity, high aspect ratio, stable design (high static margin), high maximum lift coefficient, low structural part count, low wing bending, and high output motor.

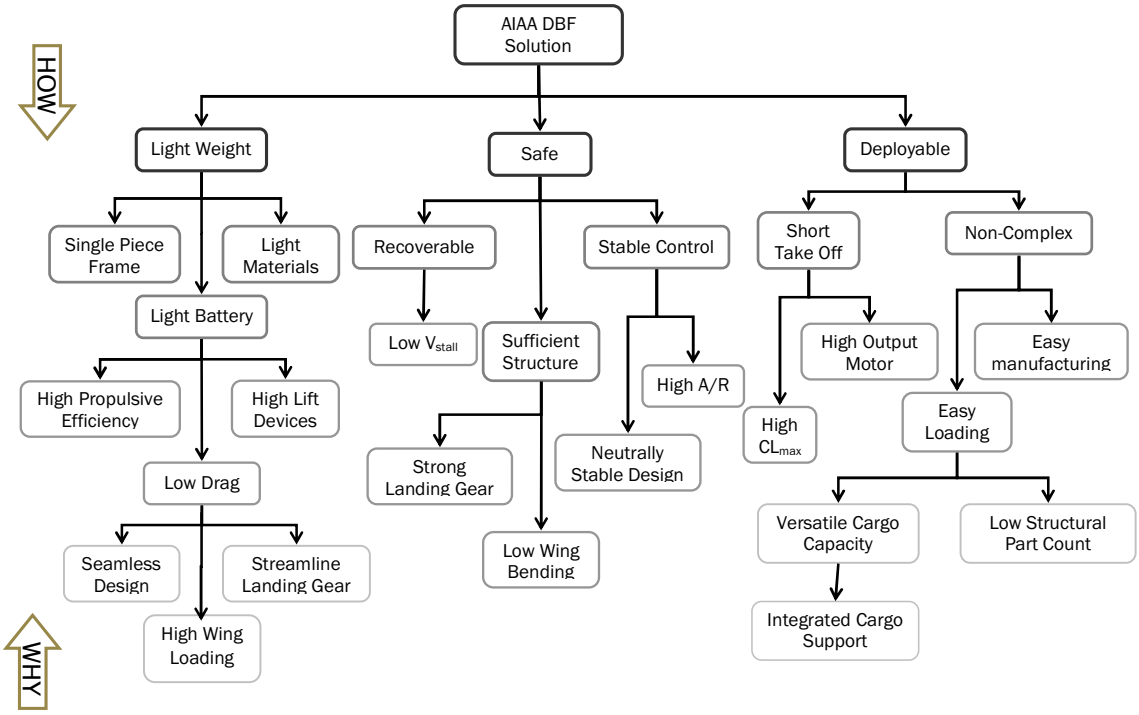

Figure 3.5: Objective Tree

3.2.2 Quality Function Deployment

Quality Function Deployment (QFD) [2] was used to establish the important design solutions to the requirements of the competition. Four main requirements were established: light weight, safe, deployable, and aerodynamically efficient. Each of these were broken down into sub-categories and compared with the engineering design solutions. The compatibility of each requirement to the different design solutions was scored on how well the requirements correlated. A scale of 9 points for a strong correlation, 3 for moderate, and 1 for weak was used. With the requirements ranked in order of importance, the most important design features and most achievable requirements were determined. It was found that a high maximum lift coefficient (C_{Lmax}), low drag, low stall velocity, and high aspect ratio were the most important design features. The requirements most readily achieved were recoverability, short takeoff, light battery, and high range. The QFD matrix is shown in Figure 3.6.

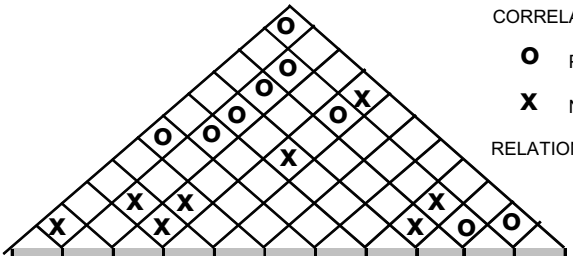

Orientation													
increase (+) decrease (-) target (o)			Engineering Characteristics (EC's)										
			+	-	+	+	+	-	-	-	+	+	-
Requirements (CR's)		Customer Importance	Aspect Ratio	Aircraft Drag	Motor Output	Wing Loading	Propulsive Efficiency	Structural Part Count	Static Margin	V_{stall}	Cl_{max}	Load Factor	Wing Deflection
Light Weight	Light Battery	10	9	9	1	0	9	0	0	0	0	0	0
	Light Materials	8	0	9	0	0	0	1	0	0	0	0	0
Safe	Recoverable	10	0	0	0	0	0	3	9	9	9	3	1
	Stable Control	6	3	0	0	0	0	0	9	3	0	0	1
	Sufficient Structure	9	0	0	0	0	0	9	0	0	0	0	9
	High Wing Strength	7	1	0	0	9	0	0	0	0	0	9	9
Deployable	Short Take-off	10	3	3	9	0	0	0	1	9	9	0	0
	Fast Loading	9	0	0	0	0	0	3	0	0	0	0	0
Aerodynamic	High Range	5	9	9	1	0	9	0	3	0	1	0	0
	High Speed	5	0	9	9	0	1	0	1	0	0	9	1
	Maneuverability	4	3	0	3	3	0	0	0	0	9	9	3
Absolute Importance			157	192	112	75	90	146	154	198	216	129	172
Relative Importance			9.6	12	6.8	4.6	5.5	8.9	9.4	12	13	7.9	10
Units of Engineering				lbf	Wh	lbf/oz^2		#	ft	ft/s		g	ft

Figure 3.6: QFD Matrix

3.3 Concept and Configuration Generation

3.3.1 Brainstorming

Using results from the Objective Tree and the QFD matrix, the members of the team independently created conceptual design sketches, as shown in Figures 3.7 – 3.9, to satisfy mission requirements and include key design features. These sketches identified various plausible aircraft configurations which were then organized into an affinity diagram and further explored during conceptual design.

3.3.2 Concept Generation

Before applying the concept selection methods, the team considered the possibility of grouping the numerous concept drawings. Several aspects of the design concepts serve as the basis for groups, such as general layout (configuration), design and performance characteristics, damage tolerance, and fabrication methods. Three major planform-based categories were devised, including the blended wing body (BWB), joined wing, and conventional configuration, as shown in Figures 3.7 – 3.9 respectively.

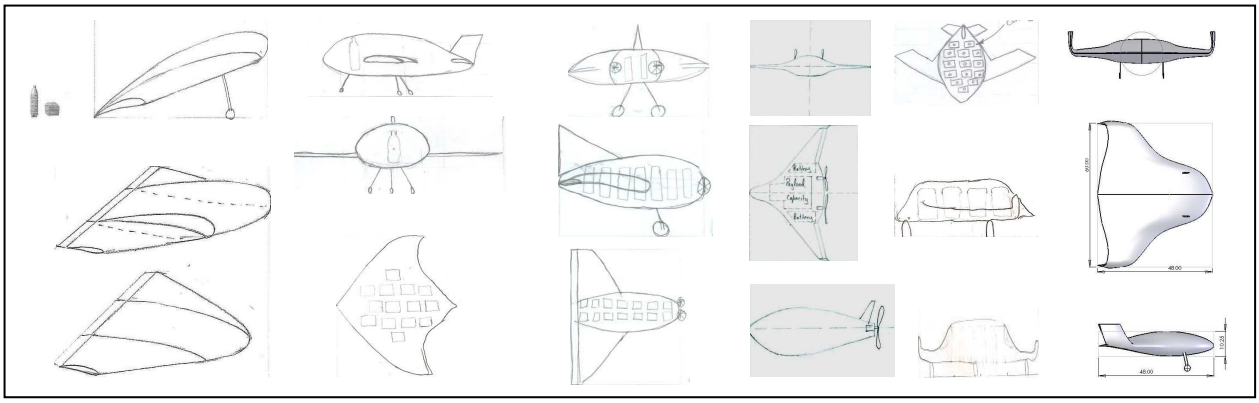

Figure 3.7: Blended Wing Body (BWB) Configurations

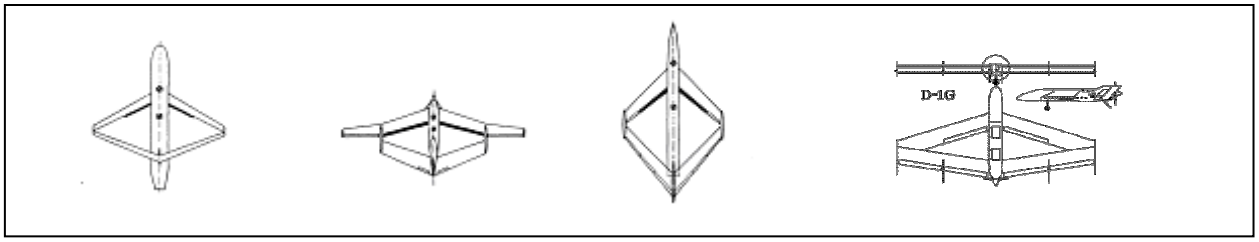

Figure 3.8: Joined Wing Configurations

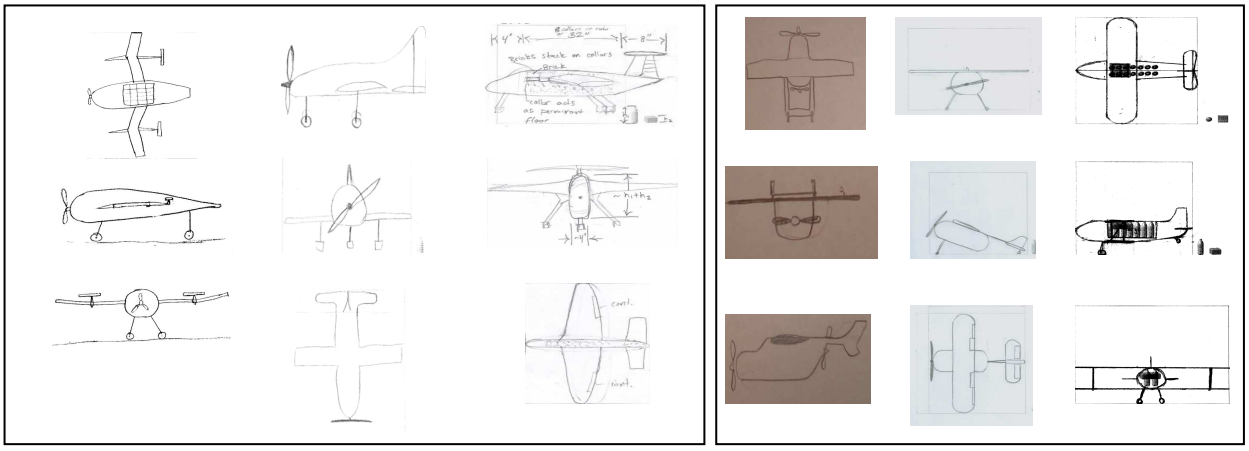

Figure 3.9: Conventional Configurations

3.4 Concept Selection

Mission modeling analysis and careful study of the rules showed that maximizing the score depended on several design requirements. The primary factor for Mission 1 is the number of laps compared to the weight of the battery. The payload loading time, battery weight, and structural weight are the score determining factors in Mission 2. To perform best in this mission, the plane should be configured to minimize loading time, thus maximizing score. It was determined that maximizing the wing span of the aircraft aided in carrying the weight of the payloads as well as increasing Mission 1 score.

3.4.1 Figures of Merit

Six figures of merit (FOM) were determined based on experience and were weighted based on relative impact on mission scores. The FOM and their description are listed below in order of importance.

1. **RAC**: Rated Aircraft Cost (RAC) was weighted highest because of its direct impact on the payload mission score, which contributes to the majority of the flight score.
2. **Payload**: The aircraft configuration affects the placement of the payload and greatly affects the load time of the payloads. It was weighted second only to RAC.
3. **Drag:** Drag limits the maximum speed attainable in Mission 1. It also affects battery weight for both missions, since larger propulsion systems are required to counteract drag. Hence, drag was determined to be of equal importance to the payload placement.
4. **Stability:** Stability was an important consideration since an unstable aircraft is difficult or impossible to fly. However, a marginally stable aircraft can still be flown with gyroscopes and pilot training, so it was weighted under payload and drag.
5. **Construction:** Complexity of the design can increase weight without providing proportional performance improvement. Hence, simplicity was emphasized.
6. **Risk:** The unknowns of a design can lead to wrong assumptions and unexpected problems. This can cause delays and increase weight, leading to redesign.

3.4.2 Weighted Objectives Method

Based on the Weighted Objectives Method [3], configuration options deemed feasible for integration into the aircraft design were contrasted using FOM. Each relevant FOM was assigned a numerical value of 1, 0, or -1 based on its positive, neutral, or negative benefit to the design, respectively.

3.4.3 Wing Configuration

The conventional monoplane is a single wing configuration used as the baseline for the wing type selection. A blended wing body can decrease parasite drag, increasing performance for the delivery mission, but the complex, smooth geometry makes construction and optimization difficult. The biplane's primary aerodynamic advantage is decreased induced drag, but with an increase in interference drag. The joined wing also decreased induced drag and increased lift but has a large risk factor associated with optimizing wing geometry to obtain drag savings [4]. This selection matrix is provided in Table 3.1.

Table 3.1: Wing Configurations Decision Matrix

Figure of Merit	Weight	Conventional	Joined	Blended	Biplane
RAC	0.2	0	0	-1	-1
Drag	0.2	0	1	0	-1
Stability	0.2	0	0	-1	0
Construction	0.2	0	-1	1	-1
Risk	0.2	1	-1	-1	0
Total	1	0.2	-0.2	-0.4	-0.6

3.4.4 Tail Configuration

Meeting the requirements of minimum drag, nominal stability, and easy construction, a conventional design was used as the baseline for comparison between the tail types. The V-tail was considered to be slightly more aerodynamically efficient than a conventional tail due to smaller surface area, however, it requires more structure due to concentrated loads and induces roll with rudder inputs [5]. The T-tail is normally used to provide extra ground clearance, or to keep the tail from being blocked by the wing and to reduce drag; however it is much heavier due to the structural requirements from the horizontal component of the tail. A canard offers a more flexible CG location and a positive component of lift but is difficult to design. A tailless configuration consisting of only the vertical appendage of a tail and no control surfaces had the main disadvantage of a complicated design. Since the driving factors are minimizing drag and RAC, the selection matrix, as shown in Table 3.2, favored a conventional design.

Table 3.2: Tail Configurations Decision Matrix

Figure of Merit	Weight	Conventional	V-tail	T-tail	Canard	Tailless
RAC	0.3	0	-1	-1	0	1
Drag	0.25	0	1	0	1	1
Stability	0.25	1	0	1	-1	-1
Construction	0.1	0	-1	-1	-1	0
Risk	0.1	0	-1	0	-1	-1
Total	1	0.25	-0.25	-0.5	-0.2	0.2

3.4.5 Landing Gear Configuration

RAC and drag, as well as the ability to rotate quickly, were important factors in the landing gear configuration selection. Compared to a tricycle configuration, the tail dragger configuration allows for decreased drag and lower weight due to a smaller 3rd wheel and eases takeoff rotation. However, propeller clearance makes it harder to have a pusher design and poor tail wheel stability requires higher pilot skill. A bicycle gear has a tandem main pair of wheels and wheels at the wingtips, which increase aircraft structural requirements and hence weight. The takeoff distance is also affected because the rear wheel in the tandem configuration tends to be far back, making it harder to rotate. The selection matrix in Table 3.3 indicates the tail dragger configuration is the best option.

Table 3.3: Landing Gear Configurations Decision Matrix

Figure of Merit	Weight	Tail Dragger	Tricycle	Bicycle
RAC	0.4	1	0	0
Drag	0.2	1	0	-1
Stability	0.2	-1	1	0
Payload	0.1	0	0	0
Takeoff Distance	0.1	1	0	-1
Total	1	0.5	0.2	-0.3

3.4.6 Motor Placement and Number

Primary factors again were RAC, payload placement, risk of propeller strikes, and off-center thrust lines. A single tractor provides the lightest weight and good propeller clearance. A single pusher also has the benefit of a lightweight power system, but leads to problems with prop clearance. This requires either heavier tricycle gear or mounting the propulsion system higher up on the back of the plane, increasing weight for the supporting structure. A pod-mounted power system achieves the needed propeller clearance, however the increase in the weight and decreased stability make pod-mounting an unfavorable option. A twin tractor may be heavier than a single engine configuration as well as requiring additional control considerations in the event of an engine failure. Based on minimizing weight and complexity, the selection matrix in Table 3.4 clearly identified the single tractor configuration.

Table 3.4: Motor Location Configurations Decision Matrix

Figure of Merit	Weight	Single Tractor	Single Pusher	Pod	Twin Tractor
RAC	0.45	0	0	-1	-1
Payload	0.35	0	0	-1	0
Risk	0.2	1	-1	-1	1
Total	1	0.2	-0.2	-1	-0.25

3.4.7 Final Configurations

It was concluded that there was insufficient data to narrow the configuration selection to a single design. Therefore, the two different configurations shown in Table 3.5 were to be carried through the preliminary design phase for further investigation and analysis. These included the conventional (BoilerBus) and blended wing body (BWB) designs. The joined wing was eliminated mainly due to the risk factor and complex construction, given the significant time constraint. The BWB incorporated a tailless design as a result of the plane's unique shape, while the conventional design maintained a conventional tail.

Table 3.5: Final Configurations

Wing Configuration	Tail	Landing Gear	Motor Location
Conventional (BoilerBus)	Conventional	Tail Dragger	Single Pusher
Blended Wing Body (BWB)	Tailless	Tail Dragger	Single Pusher

3.5 Conceptual Design Conclusion

Conceptual design began by evaluating the mission rules and identifying key design requirements and feasible configurations. Scoring analysis concluded that the aircraft weight and loading time were the key design drivers. The weighted objectives method was used to narrow design configurations to two conceptual designs; the conventional monoplane (BoilerBus) and the blended wing body aircraft (BWB).

4 PRELIMINARY DESIGN

4.1 Preliminary Design Methodology

The goals of preliminary design were to size the aircraft chosen during the conceptual design and to identify the optimal configuration on the basis of simulated mission performance/scores. Preliminary design was accomplished in several phases as depicted in Figure 4.1

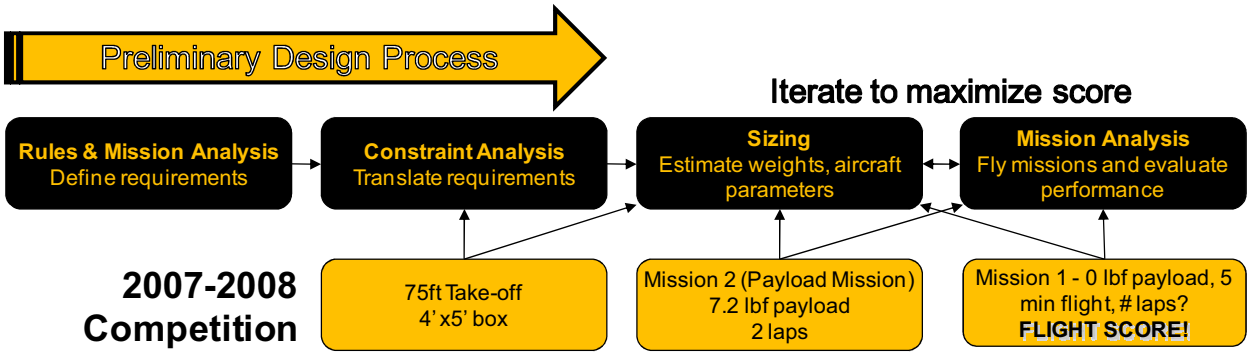

Figure 4.1: Preliminary Design Methodology

Design requirements were translated to a bounded design space through the creation of a constraint analysis program in MATLAB, as shown in Figure 4.2. Aircraft and mission specific parameters such as aspect ratio and desired maximum speed are used as program inputs. The program output is in the form of a mission constraint diagram, relating specific power to wing loading for each critical phase of flight. The specific power and wing loading coupling is then used as an input into a weight and scoring calculation program, which determines the aircraft weight and effectively flies each mission to compute a mission score. This was then used as a tool to size the aircraft in the sizing trade analysis.

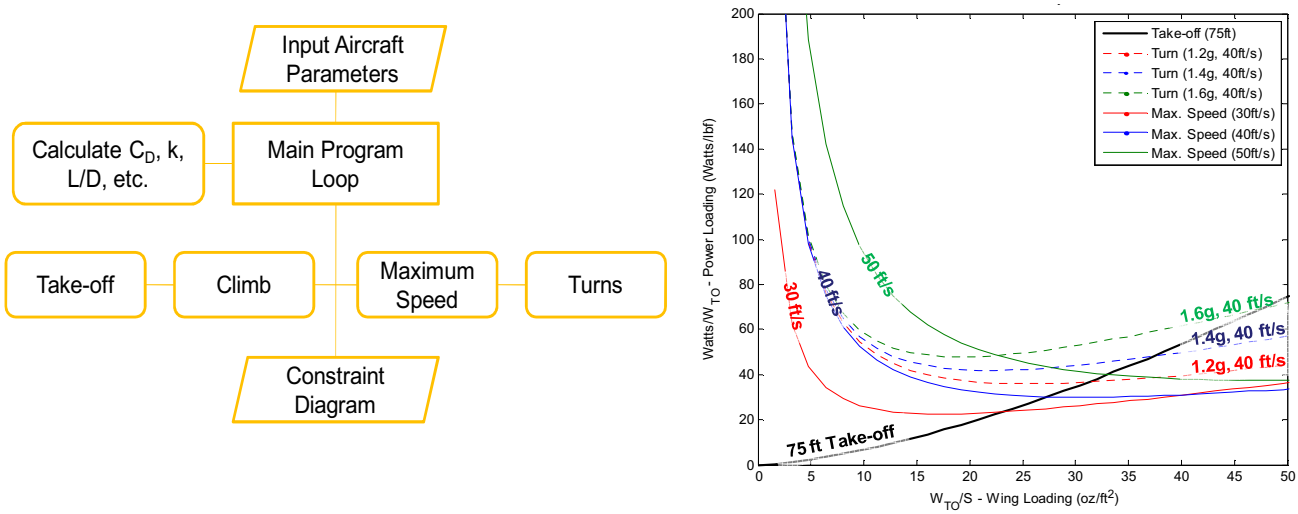

Figure 4.2: Mission Constraint Analysis

4.2 Initial Mission Model

Using aircraft performance equations from Brandt[6] and Raymer[7], a sizing and scoring analysis program was created in MATLAB for the determination of the aircraft empty weight, battery weight, gross take-off weight, and mission scores. The program iterates through aircraft aspect ratios, number of laps for Mission 1, and wing loadings with corresponding power-to-weight ratio, as determined from the constraint analysis. Each aircraft was sized to meet take-off and flight course requirements, and aircraft weights are computed based on the energy requirements for each phase of flight [8]. Through the iterative process, the feasible design space was constrained by a stall speed constraint of 44 ft/s to maintain reasonable approach speeds, a wing span of 5', and a Mission 1 flight time of 5 minutes. Overall flight score was maximized to obtain the final aircraft sizing parameters. A simplified flowchart of the analysis can be seen in Figure 4.3.

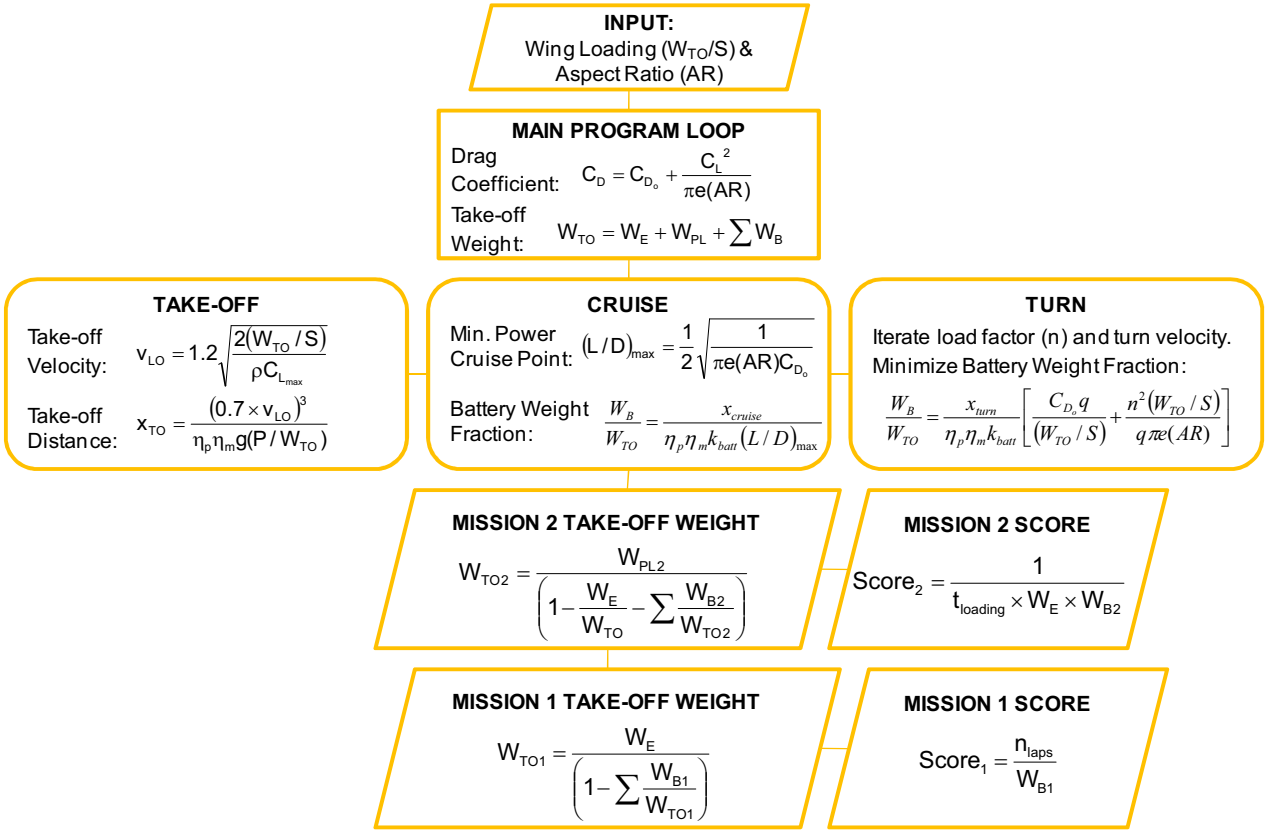

Figure 4.3: Aircraft Sizing Flow Chart

The empty weight fraction (W_E/W_{TO}) used to compute a mission take-off weight was empirically derived from previous competition aircraft data. Battery weights were related to their energy output using the specific battery energy density constant (k_{batt}) computed from manufacturer data. Motor and propeller system efficiencies (η_m and η_p) were assumed to be constant. All such preliminary estimates are shown in Table 4.1. These estimates were updated during the course of design, based on actual test data.

Table 4.1: Preliminary Sizing Estimates

Parameter	Preliminary Estimate	Source
Zero Lift Drag (C_{Do})	0.08	Conservative Historical Estimate
Oswald's Efficiency Factor (e)	0.65	
Propeller Efficiency (η_{prop})	0.6	
Motor Efficiency (η_{motor})	0.6	
Maximum Lift Coefficient (C_{Lmax})	1.2	
Battery Energy Density (K_{batt})	100000 J/lbf	Empirical Data
Empty Weight Fraction (W_{Empty}/W_{TO})	0.4	
Mission 1 Payload Weight ($W_{payload1}$)	0 lbf	Mission Requirements
Mission 2 Payload Weight ($W_{payload2}$)	7.2 lbf	
Competition Field Elevation	1300 ft MSL	

The first phase of sizing was used to quantify and compare performance of conventional and blended wing body aircraft. Both aircraft were sized for maximizing range while meeting take-off requirements. Initially, turns were considered as a part of cruise and were not fully accounted for in the sizing calculations. With the conventional design, the addition of flaps was assumed, improving the maximum lift coefficient of the aircraft from 1.2 to 1.88 as determined using equations from Raymer[7]. This helped alleviate wing loading restrictions imposed by the takeoff constraint of 75'.

In the case of the blended wing body aircraft, the fuselage lift contribution was accounted for in the aspect ratio calculations. The coefficient of zero-lift drag (C_{Do}) was also assumed to be lower than that of a conventional design since S_{wet}/S is estimated to be lower in the case of blended wing body aircraft. Since the payload height, width, and weights are defined, both aircraft were designed around these constraints.

Table 4.2 compares the aircraft sized for maximum scoring for both designs. The use of flaps in the conventional design helps substantially increase the aspect ratio of the aircraft and the corresponding flight score. In the case of the BWB aircraft, the aspect ratio is intrinsically constrained by the design and the 4' x 5' size limitation. However, based on an estimation of lower zero-lift drag, high scores for relatively low aspect ratios are obtainable.

Table 4.2: Comparison of Conceptual Designs

	BoilerBus1	BWB
Mission 1 Max Score	10.98	10
Mission 2 Max Score	0.43	0.4
Aspect Ratio	10	2.4
Span (ft)	5	5
Chord (ft)	0.5	Variable
Mission 2 Wing Loading (oz/ft^2)	80	19.8
Empty Weight (lbf)	5.11	5.14

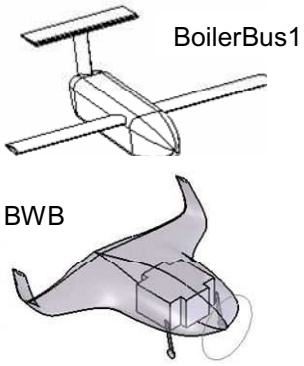

4.3 Sizing Trades

Initial trade-studies were limited to evaluating aircraft sized for best range. Aircraft sizing was refined to include a complete flight simulation for each mission, inclusive of turns, which were found to be a major contributor to flight distance. The initial basis for this analysis was an evaluation of maximizing score by minimizing battery weight, i.e. energy requirement, for all segments of flight for Mission 2. Aircraft aerodynamic characteristics that were computed using preliminary estimates based on previous wind tunnel data. Energy requirements for each mission leg are shown in Figure 4.4.

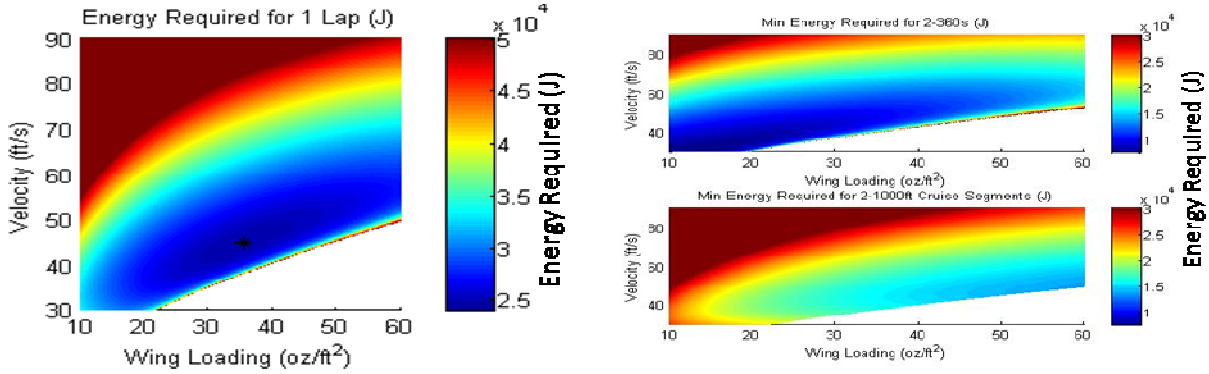

Figure 4.4: Comparison of Turn and Cruise Energy Requirements for Mission 2

Figure 4.4 shows that minimizing energy requirements, and hence maximizing score, for each mission segment creates conflicting design requirements. An aircraft optimized for cruise would require higher wing loading and have a higher aspect ratio, whereas lower wing loading and aspect ratio is optimal for turning. Combining analysis for both cruise and turn yields the target design space for the aircraft for the payload mission. For Mission 2, aircraft wing loading should fall in a range between 30 and 40 oz/ft^2 and the aircraft should operate at optimal mission speeds between 40 and 50 ft/s.

4.4 Revised Mission Model

The aircraft sizing logic was updated to more accurately incorporate all segments of the flight simulation. The empty weight fraction was reduced from the competition average to 0.23, as determined from the most competitive historic competition aircraft. The impact of motor weight as a function of maximum power requirements was also taken into consideration using manufacturer data, along with fixed sizing requirements for the fuselage based on payload requirements. Estimations for Oswald's efficiency factor were increased to 0.71 and maximum lift coefficient was increased to 1.5 based on wind tunnel testing results of similar aircraft. Using the updated aircraft constants and maintaining all design constraints, the sizing simulation was rerun for a conventional design with the feasible design space as shown in Figure 4.5. Balancing cruise and turn performance while meeting take-off requirements, the optimal scoring design was shown to lie on the edge of the feasible design space. Since the geometry of the BWB was

fixed by the payload constraints, the addition of the turns to the mission analysis was found to be negligible. Thus, the results for the refined mission analysis are shown only for the BoilerBus1 design.

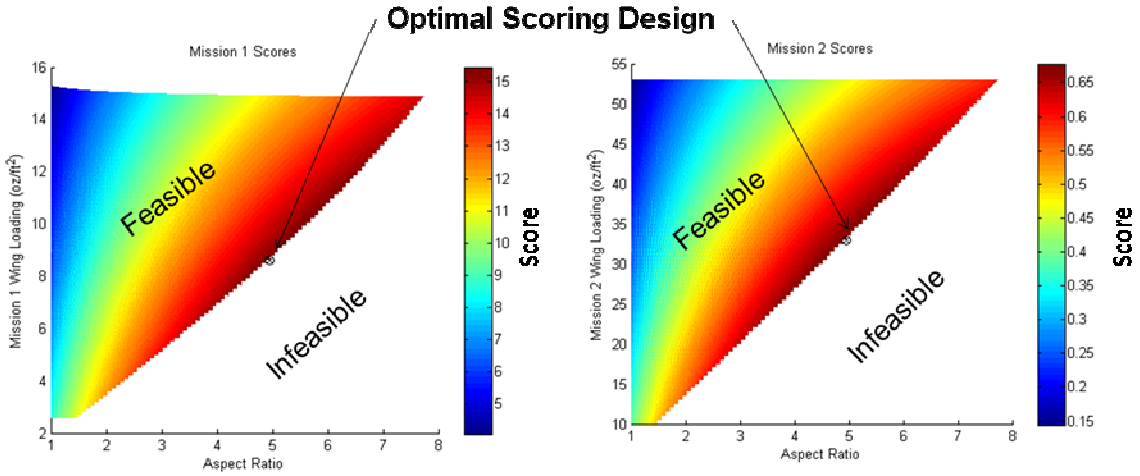

Figure 4.5: Feasible Design Space for a Conventional Design

The refined configuration of the BoilerBus1 aircraft, as shown in Figure 4.6, was determined to have an aspect ratio of 4.8, a chord of 1.1', wing loading of 32 oz/ft^2, and an empty weight of 2.65 lbf. Uncertainties in the mission model arise from certain basic simplifying assumptions made. Acceleration at take-off is approximated by using an average velocity estimated at 70% of the velocity at lift-off. The climb segment of flight is ignored, and cruise and turn segments are also assumed to be at constant velocity. Lastly, the flight simulation does not account for human error, leading to partial off-design flight. Based on the results of the aircraft sizing and performance, both designs appeared to be viable, competitive options and were therefore manufactured and tested at full-scale

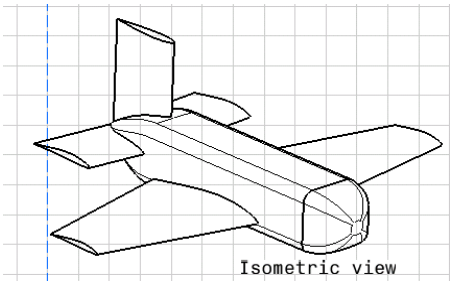

Figure 4.6: Updated BoilerBus1

4.5 Design Trades

4.5.1 Aerodynamics

Preliminary aerodynamic analysis was conducted in order to select an airfoil for each design option and estimate aircraft coefficients of lift, drag, and moment.

4.5.1.1 Airfoil Selection

During preliminary analysis, XFOIL, a 2D panel method solver, was used as the primary tool for analyzing a large set of airfoils. Preliminary airfoil selection was based on the comparison of drag polars (C_l vs C_d) and lift curves (C_l vs α), while noting the moment coefficient (C_m). Using the Reynolds number computed in the mission profile, two-dimensional airfoil performance data was obtained using the XFOIL viscous flow solver. The resulting drag polars and lift curves for the best performing subset of the airfoils for the wing of the conventional aircraft is provided in Figure 4.7. The Clark Y airfoil was chosen for preliminary design and construction due to its simple geometry. Further airfoil selection is conducted in the detail design.

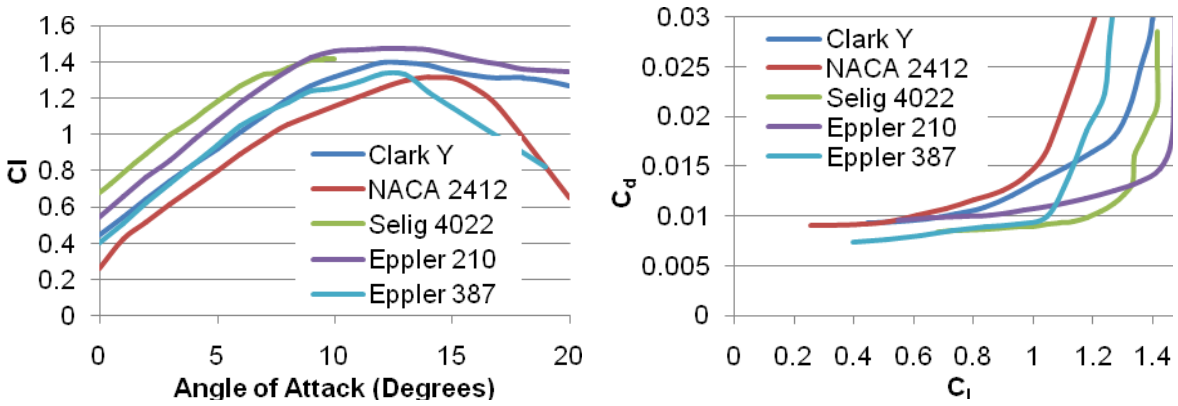

Figure 4.7: Conventional Aircraft Airfoil Selection Using XFOIL

Similar selection of the airfoil for the BWB was conducted using XFOIL. A minimum thickness for the airfoil was determined to be 21% in order to accommodate the payload. Seventeen NACA airfoils that matched the minimum thickness requirement were analyzed. An additional consideration for this airfoil was to balance the large pitching moment generated by the fuselage lifting-body. Two solutions considered were to use a reflexed airfoil and/or to use different airfoils at the aircraft centerline and tip. Based on these requirements, the NACA 654-421 was chosen for its lower drag coefficients at higher lift coefficients.

4.5.1.2 Aircraft Analysis

Computational Fluid Dynamics (CFD) was used to obtain a Navier-Stokes solution for the complete aircraft using the modeling methodology depicted in Figure 4.8. Full-scale aircraft geometry was modeled in the CATIA CAD package and simplified by excluding the landing gear. Taking advantage of the longitudinal symmetry, only half of the fluid domain was modeled to improve solver run time. The 'clean' CAD model was discretized using the GAMBIT mesh generation package. The flow solution was obtained using FLUENT and post-processed using Tecplot after conducting a convergence study to evaluate solution accuracy.

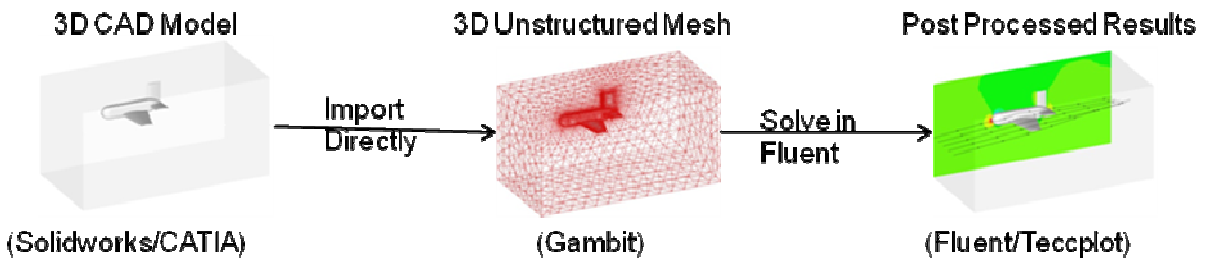

Figure 4.8: 3D CFD Analysis Methodology

In order to easily conform to the aircraft geometry, the computational mesh consisted of a triangular surface mesh on the aircraft and an unstructured tetrahedral volume mesh as shown in Figure 4.9.

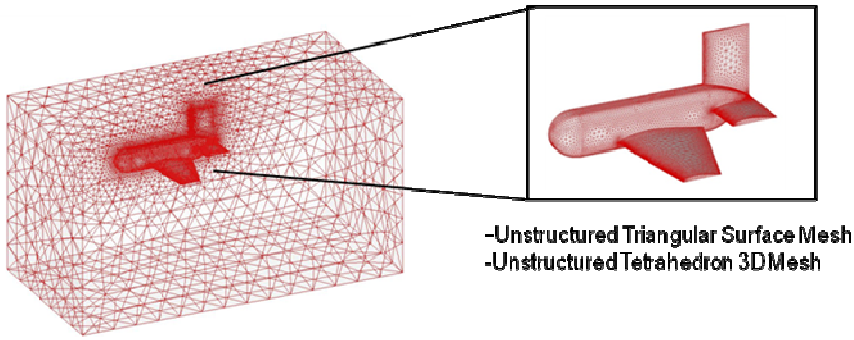

Figure 4.9: Conventional Aircraft 3-D Mesh

Viscous, 2nd order accurate, steady state flow solutions were obtained for angles of attack ranging from -5° to 20°, at the Reynolds number used for the wind tunnel tests. As shown in Figure 4.10, the computational results for both the BoilerBus1 and BWB were compared to the wind tunnel testing results, which are further discussed in Section 8.2.1.

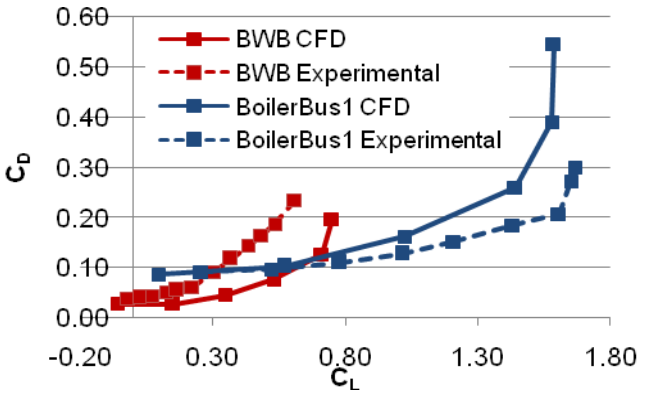

Figure 4.10: Wind Tunnel and CFD Results

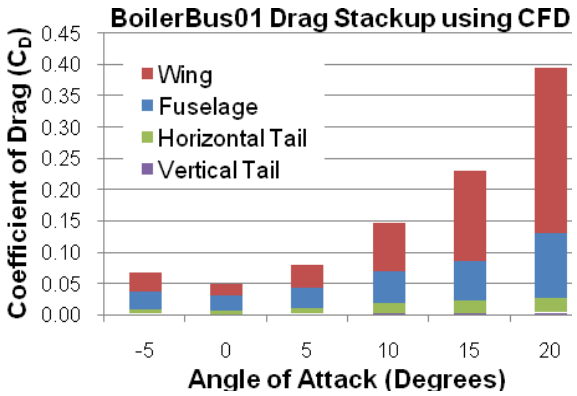

Figure 4.11: Prototype Aircraft Drag Breakdown

As expected, the BWB aircraft had lower zero lift drag, however the design is greatly limited by a small operating envelope with poor take-off and cruise performance. This conflicts with the design requirements and resulted in the elimination of the BWB design. Aerodynamic data obtained from wind tunnel tests of the BoilerBus1 was used to validate lift and drag predictions from the preliminary CFD model. The CFD

results accurately predict zero-lift drag but deviate from experimental results at higher angles of attack due to limitations simulating laminar flow. The drag breakdown by component for the BoilerBus1 is summarized in Figure 4.11 and was obtained from preliminary CFD. It was used to identify the primary targets for aerodynamic optimization in detailed design.

4.5.2 Stability

The stability of the preliminary design aircraft was conducted using historic aircraft sizing data and a MATLAB Simulink model encompassing all relevant facets of vehicle stability and control.

The tail was sized following the empirical method outlined in Raymer[7]. Tail volume coefficients were defined by the product of the tail moment arm and the planform area divided by the product of the wing span and wing planform area. These values were taken from empirical data and were 0.08 for the vertical tail and 1 for the horizontal tail. Another standard assumption included a 60% fuselage length for the moment arm. The resulting tail sizes are given in Table 4.3.

Table 4.3: Tail Sizes

	Vertical Tail		Horizontal Tail	
	Chord (ft)	Span (ft)	Chord (ft)	Span (ft)
BoilerBus1	0.417	1.00	0.347	1.50
BWB	N/A	N/A	N/A	N/A

The control surfaces were sized in a similar fashion. Ratios of control surface chord to wing chord were taken from empirical data. These values are 0.20 for the aileron, 0.45 for the elevator, and 0.40 for the rudder. The resulting control surface sizes are given below in Table 4.4. These sizes were increased for prototype construction to ensure adequate control authority and compensate for any sizing errors.

Table 4.4: Control Surface Sizes

	Rudder		Elevator		Ailerons	
	Chord (ft)	Span (ft)	Chord (ft)	Span (ft)	Chord (ft)	Span (ft)
BoilerBus1	0.200	0.900	0.100	2.00	0.225	1.35
BWB	0.600	1.84	0.488	2.00	0.488	2.00

4.5.3 Structures

4.5.3.1 Preliminary Considerations

For the BoilerBus1 and BWB design, many structural considerations were evaluated. The ease of manufacturing, the ease of structural analysis, and preliminary structural benefits versus structural drawbacks in the design were areas of primary focus. When considering the manufacturing of each aircraft, the material expense, manufacturing time, and the required processes were taken into account. To determine the ease of structural analysis with different finite element analysis packages, a qualitative

approach was followed on the required internal structure. Structural benefits and drawbacks included the weight and strength achievable in each design.

4.5.3.2 Blended Wing Body Design

Structurally, the BWB's only significant advantages are a smaller bending moment on the wings due to lower wing loading and a reduced stress concentration on the wing joint with the body since the entire aircraft acts as a wing. The main considerations for manufacturing techniques were either a composite shell made using a mold or creating the aircraft out of a solid piece of EPS foam using a 5-axis CNC machine and then covering it with a thin composite layer. For the foam bodied design, some balsa control surfaces were required in order to have adequate strength. The structural analysis was done in CATIA using its finite element package, called Generative Structural Analysis. This analysis was conducted by applying a point force on the wing tips and pinning the fuselage of the aircraft. This was only a validation model as the material properties are not representative of the actual aircraft built but the stress concentrations are still valid. The composite shell option was also investigated. In this analysis, the aircraft has a spar that runs through the mean chord line of the aircraft. During this analysis, the aircraft was pinned on its axis of symmetry and a uniform pressure distribution was applied on its wing surface. This was only a validation analysis. Figure 4.12 shows the results of the preliminary BWB structural analysis for both the composite shell and solid foam design options.

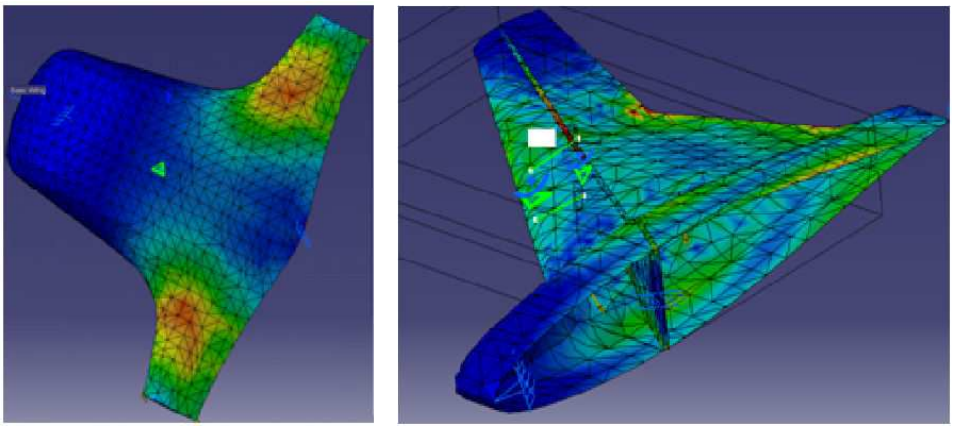

(a) Solid Foam (b) Hollow Compsite Shell with Spar

Figure 4.12: Preliminary BWB Stress Analysis

4.5.3.3 Conventional Design

The conventionally designed aircraft had no significant structural advantages when compared to the blended wing body. However, with a conventional design there are more degrees of freedom to optimize the structural properties such as the wing location, wing sweep, and the tail design. Also, more empirical data is available for the conventional design to compare the structural analysis results and it is the most successful design in production.

Manufacturing of the BoilerBus1 aircraft is relatively easy due to its simple design. For wing manufacturing, the three main material options considered were balsa covered foam wings, hollow composite wings, and traditional web and spar covered wings. In CATIA's Generative Stress Analysis Workbench, simple FEA was conducted on the BoilerBus1 wing. The wing was modeled as a hollow composite shell. The wing root was pinned, while a point force was applied to the wing tip. Results from the analysis are shown in Figure 4.13. Once again, the material properties are not correct, but the stress concentrations are accurate.

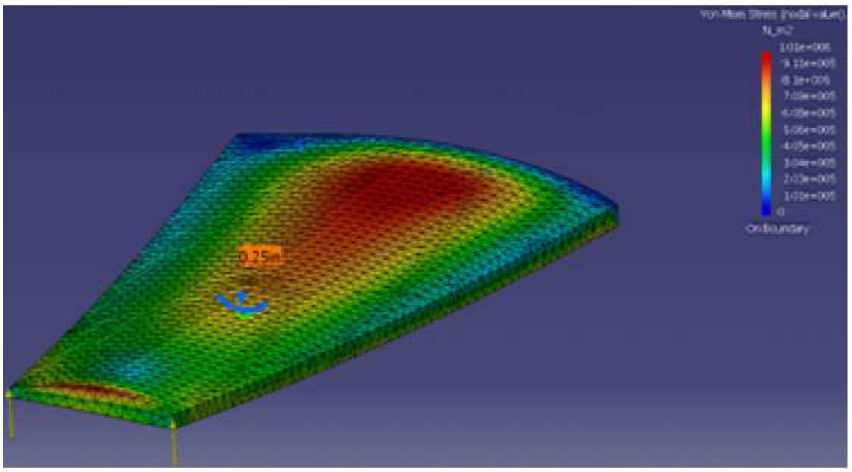

Figure 4.13: Preliminary Conventional Aircraft Stress Analysis

4.5.3.4 Material Selection

The objective of the material analysis was to build a strong yet light aircraft. This task would be achieved not only by trying different construction and design techniques but also through the use of more exotic composites rather than previously tried and tested materials. The more common materials used in model aircraft construction include fiberglass/epoxy, balsa, foam and carbon fiber/epoxy. These materials perform well, providing good rigidity and strength while minimizing weight. However, through research into commercially available composite materials, Rohocell and honeycomb were viewed as possible core material options that would provide a further reduction in weight.

The thinnest of these materials available from the manufacturer was found to be 1/8", which is adequate for its intended use. It was envisioned that the core materials would be used in a sandwich type structure in between thin layers of Aramid Kevlar epoxy, which would form the outer surfaces. This sandwich structure would make up the wing structure, providing adequate strength for mission purposes while dramatically reducing weight.

4.5.4 Aircraft Performance

Estimated aircraft mission performance is presented in Table 4.5, based on the results of preliminary aircraft sizing for maximizing aircraft mission scores.

Table 4.5: Aircraft Performance for BoilerBus1

Performance Summary								
Mission #	**Laps #**	**W_{TO}/S (oz/ft^2)**	**P/W_{TO} (Watts/lbf)**	**W_{TO} (lbf)**	**$W_{payload}$ (lbf)**	**$W_{battery}$ (lbf)**	**W_{empty} (lbf)**	**Raw Score**
1	1	8	147	2.71	0.00	0.07	2.65	15.35
2	2	32	38	10.40	7.20	0.56	2.65	0.68

	Mission 1 Performance				Mission 2 Performance			
Segment	**$Power_{req}$ (Watts)**	**Velocity (ft/s)**	**Time (s)**	**Distance (ft)**	**$Power_{req}$ (Watts)**	**Velocity (ft/s)**	**Time (s)**	**Distance (ft)**
Take-off	382	20.92	0.18	3	382	40.96	2.62	75
Cruise	42	20.93	95.53	2000	313	41.00	97.57	4000
Turn	62	20.92	8.33	174	511	41.96	14.65	615
		Total	104.04	2177		**Total**	114.84	4690

4.5.5 Preliminary Design Conclusion

At the conclusion of the preliminary design phase, the aircraft design was down-selected to the BoilerBus1 design, as it appears in Figure 4.14. The BWB, as shown in Figure 4.14, had poor aerodynamic performance relative to the BoilerBus1 design. Additionally, stability and control of the BWB design was a major concern. This concludes the first design spiral, which included conceptual and preliminary design validated by the wind tunnel and flight tests. All future design considerations were focused on the optimization of the conventional design, BoilerBus1.

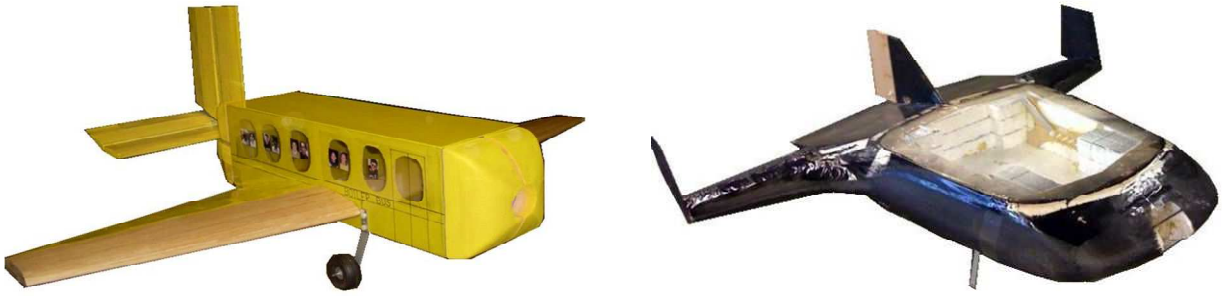

BoilerBus1 BWB

Figure 4.14: Preliminary Aircraft Designs

5 DETAIL DESIGN

The goals of the detail design were to further design and optimize the BoilerBus1 aircraft. Detail design was accomplished using the methodology as depicted in Figure 5.1. The optimized version of the BoilerBus1 aircraft was named BoilerBus2.

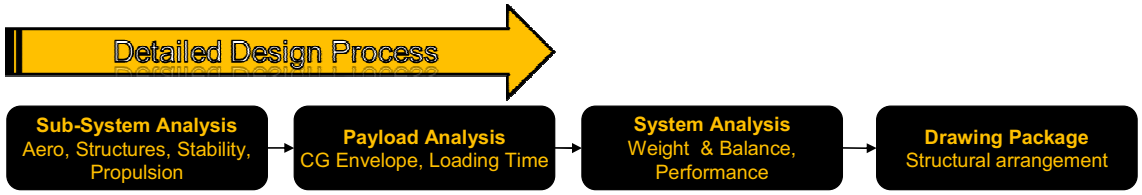

Figure 5.1: Detail Design Methodology

5.1 Payload Configuration

The objective of Mission 2 is to fly two laps of the course with any combination of the payload and to minimize system weight, battery weight, and payload loading time. Design options for the payload restraint system included several different concepts. In option one, the payload would be contained within a box with a swiveling lid. However, the payload could not be securely restrained within the box. In option two, the payload is held individually by restraints similar to a light bulb changer. This design would be capable of holding only the water bottles and could not accommodate the bricks. A third design had a board with holes and a net covering. The water bottles would be dropped into the holes to hold them in place, and the bricks would be placed on top of the board. A net would keep the payload from moving. The design was eliminated from consideration due to the large amount of loading time it required.

The final constraint system decided upon was a design in which bottles are placed in 8.75” x 4.125” x 4.125” compartments and bricks are placed in 2.75” x 4.125” x 4.125” slots. Between each slot for the bricks there are ¼” carbon fiber pegs to separate them. Different configurations were designed to evaluate the layout of these compartments, as shown in Figures 5.2 - 5.5. All configurations have a restraining lid, which is not shown in the diagrams to give a more clear view of the layout.

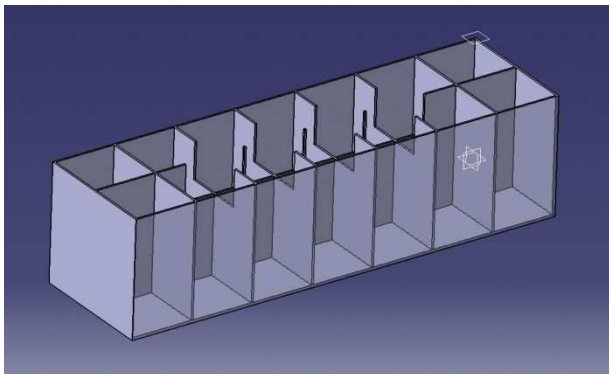

Figure 5.2: Payload Configuration A

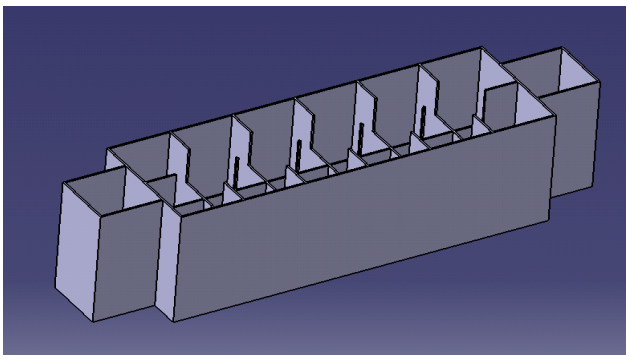

Figure 5.3: Payload Configuration B

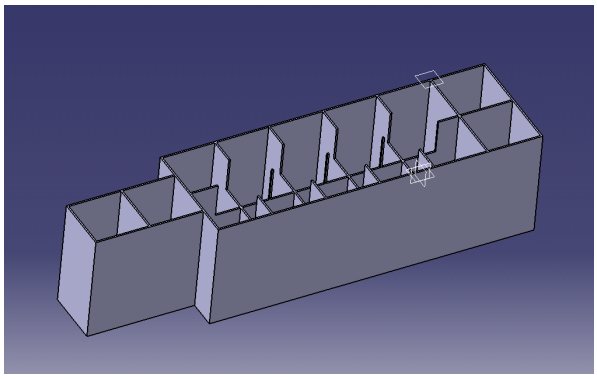

Figure 5.4: Payload Configuration C

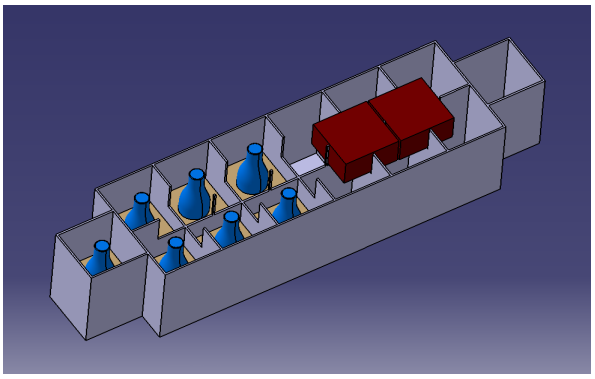

Figure 5.5: Sample Payload in Config. B

The change in the center of gravity location for the aircraft was determined for each payload combination of each configuration. An optimal payload arrangement would mean a minimal change in the center of gravity across all possible payload combinations. Table 5.1 summarizes the minimum longitudinal changes in the center of gravity for each payload combination and each configuration. A negative ΔCG denotes an aft change and positive denotes a forward change. As evident from the table, all three configurations have approximately the same maximum change in center of gravity, but each configuration has other unique characteristics, which make it more or less favorable.

Table 5.1: Payload Configurations/ Weight & Balance

	Configuration A	Configuration B	Configuration C
Payload	Minimized ΔCG	Minimized ΔCG	Minimized ΔCG
14 Bottles	0.00”	0.00”	0.29”
4 Bricks	0.00”	0.00”	0.00”
10 Bottles, 1 Brick	-0.18”	-0.24”	0.12”
7 Bottles, 2 Bricks	-0.51”	-0.48”	-0.23”
3 Bottles, 3 Bricks	-0.46”	-0.43”	0.46”
Maximum ΔCG	-.51”	-.48”	.46”

Configuration A, as given in Figure 5.2, is a symmetric envelope with two rows of seven compartments and four slots for bricks centered in the envelope. Since none of the compartments for bottles are individually centered over the center of gravity, the payload combinations with an odd number of bottles have a lateral change in center of gravity, causing rolling moments in the aircraft, reducing in-flight stability.

Configuration B, as shown in Figure 5.3, is a symmetric envelope with two rows of six compartments, and one compartment centered on each of the ends. It is necessary to have five brick slots to balance the center of gravity for the four-brick combination. Because of the configuration’s symmetry, all of the payload combinations can be arranged so that the changes in center of gravity are either forward or aft. This advantage allows for the change in center of gravity to be controlled for each payload combination.

Configuration C, as appears in Figure 5.4, is an envelope with two rows of six compartments, with two compartments centered on one end. The optimum arrangements of configuration C were only slightly better than the other two configurations, as seen in Table 5.1.

The payload is restrained identically by all three configurations. An inner lid is attached to the outside of the fuselage with hinges on one side and pivoting latches on the other. The inner lid keeps the payload contained in the event that the aircraft should become inverted. An outer hatch, which is part of the exterior of the plane, covers the payload restraint system and opens independently by latching under the edge of the inner lid. When the inner lid is opened, the outer hatch automatically opens with the lid. This method reduces loading time by requiring only one motion to gain access to the payload envelope.

Configuration B was chosen for the final aircraft design due to its superior aerodynamic performance relative to the other two configurations as discussed in Section 5.2.

5.2 Aerodynamics

In the detailed design phase, aerodynamic analysis was pursued in two phases. In the first phase, the wing and fuselage designs were analyzed separately. The second phase examined the aerodynamic performance of the complete BoilerBus2 aircraft, adding the effect of component interactions.

5.2.1 Wing Design

Wing design optimization was pursued by obtaining steady-state solutions of 3D models using the FLUENT Navier-Stokes solver and CMARC panel method solver. FLUENT predictions of induced drag are limited, so the coefficient of induced drag was determined using CMARC. Combining relevant predictions from the CMARC panel code and the FLUENT CFD yielded the total drag.

The computational domain included a single full-scale wing mounted to a flat plate at the root simulating fuselage interaction. Solutions were obtained at 5^{o}, 10^{o} and 15^{o} angles of attack to evaluate cruise and take-off performance. Incorporating 3D effects, airfoil selection was revisited by studying rectangular wings. Drag polars for the different wings identified in the preliminary design are shown in Figure 5.6.

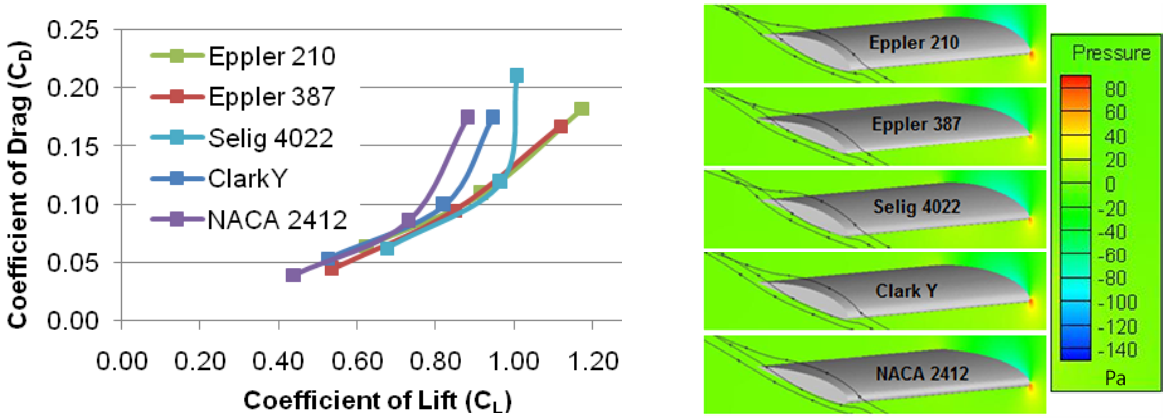

Figure 5.6: Wing airfoil analysis using CFD

The Eppler 210 and Eppler 387 airfoils were identified to have the lowest drag at lower angles of attack for cruise and relatively high lift coefficients to meet take-off and turn requirements. The Eppler 210 was chosen due to the inability to meet manufacturing tolerance on the Eppler 387.

In order to study the effects of taper ratio and dihedral on the aerodynamics of the wing, a design of experiments (DOE) was completed by analyzing the Eppler 210 wing at taper ratios of .25, .50, .75, and 1.0, and dihedrals of 0^o to 8^o. Each design case was analyzed using FLUENT at flight conditions anticipated for the payload mission to capture aerodynamic trends. A comparison of drag polars for each case revealed negligible aerodynamic impact from varying the taper ratio. As the taper ratio is decreased, there is an increase in viscous drag and a decrease in induced drag and structural bending load. At the design Reynolds number, the changes in induced drag and viscous drag nearly counteract each other. Based on Raymer[7], a taper ratio of 0.45 was chosen. Dihedral was also found to have negligible effect on aerodynamics, allowing for 3^o dihedral to be implemented for stability purposes without an aerodynamic penalty.

5.2.2 Fuselage Design

Aerodynamic design of the fuselage section was pursued in a similar fashion to the wing, by evaluating an isolated full scale 3D model using FLUENT. In order to minimize drag, the fuselage section was selected to be at 0^o angle of attack during the cruise segment of flight. Required lift of the aircraft is to be achieved by introducing an adequate angle of incidence for the wing.

Initial test configurations were generated on the basis of sizing requirements of the most size restrictive payload of 14 bottles and a longitudinal length constraint of 46”, allowing two inches for the motor extrusion from the nose. Three different fuselage configurations, as shown in Figure 5.7, were evaluated on the basis of reducing the center of gravity envelope with different payload combination and reducing fuselage drag.

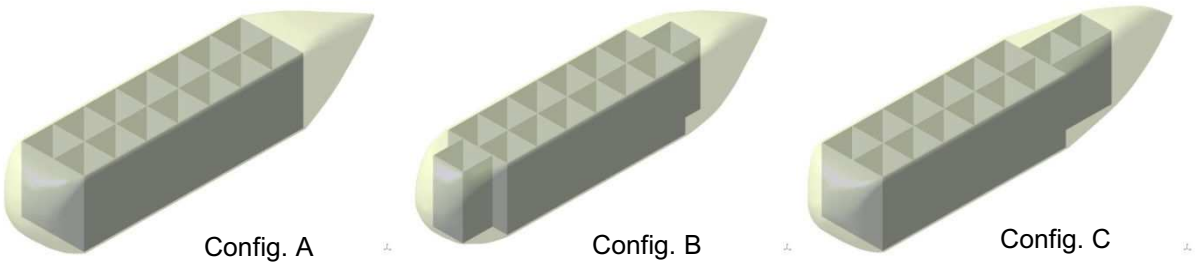

Figure 5.7: Fuselage Configurations

Computational results identified Configuration B to have the lowest drag of the baseline configurations due to its longer (than A) and more symmetric (than C) rear section. Since the aft fuselage geometry had limited restrictions because of the payload, alternative geometries for Configuration B were evaluated, as appears in Figure 5.8, to better address the 3D closure problem.

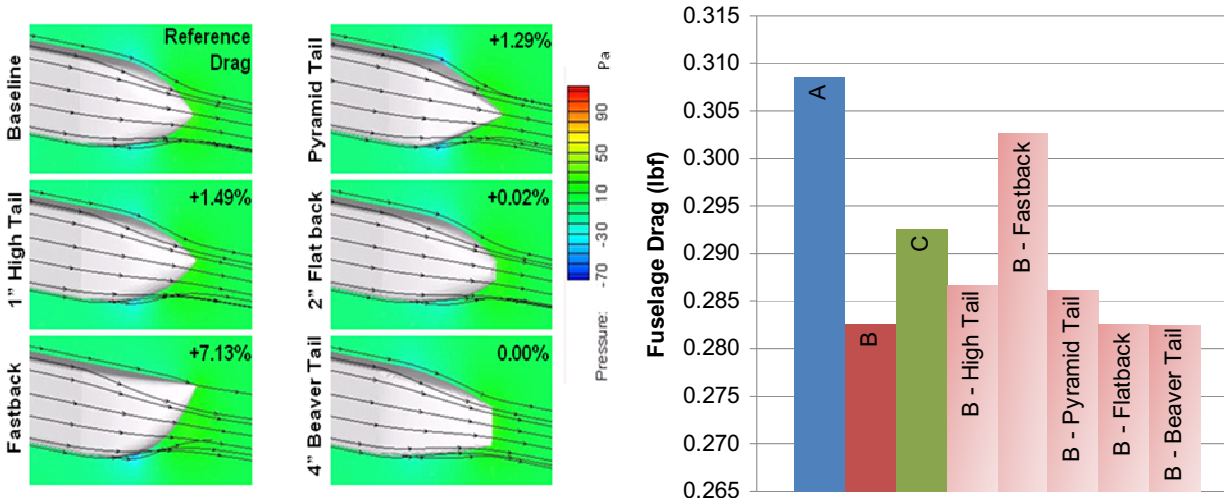

Figure 5.8: Fuselage Drag Comparison

From the fuselage drag comparison, baseline configuration B, along with its derivatives of the Flatback and Beaver-Tail were found to have the lowest predicted drag. The Beaver-Tail configuration was selected due to ease of manufacturing and possible directional stability benefits.

5.2.3 Complete Aircraft Aerodynamics

Following validation of the BoilerBus1 CFD model using the wind tunnel test results, the aerodynamic analysis of the BoilerBus2 was initiated using a similar computational model. The entire aircraft, excluding landing gear, was modeled in FLUENT and viscous, 2nd order accurate, steady state flow solutions were obtained for angles of attack ranging from -5^{o} to 15^{o}, at the Reynolds number computed for Mission 2. Based on the angle of attack for maximum L/D ratio determined from the wind-tunnel testing of BoilerBus1, the wing incidence was set to 8^{o}. This helped minimize fuselage drag by maintaining it at zero angle of attack during cruise as was validated by the analysis results shown in Figure 5.9.

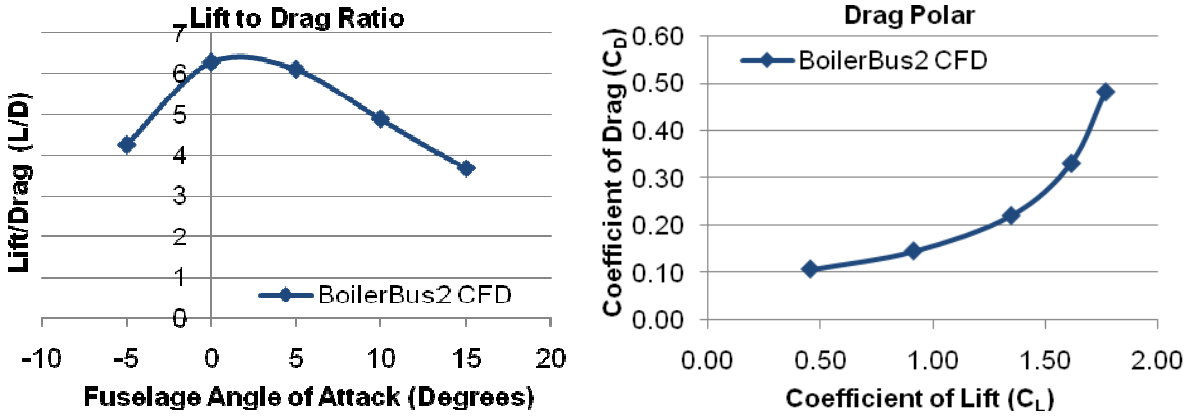

Figure 5.9: BoilerBus2 Predicted Aerodynamic Performance

A drag polar for BoilerBus2 is also shown in Figure 5.9 and is expected to be within 5% of planned future wind tunnel testing. The evolution of aerodynamic performance over the design and testing phase is discussed in Section 8.2.1 of the report.

5.3 Stability

The tail and control surface sizes for the prototype aircraft were intentionally built larger than required in order to ensure adequate control authority in the flight tests. In detail design, these sizes were optimally decreased for the lowest weight and drag possible while ensuring the stability of the aircraft.

5.3.1 Longitudinal Stability and Control

With the goal of low weight and drag, a stabilator was chosen for longitudinal control to decrease the required horizontal planform area. The first step taken to size the stabilator was determining the stability derivatives for the prototype aircraft dictated by its geometry. From these stability derivatives, a longitudinal x-plot was made to establish the static margin as a function of stabilator planform area, S_h, as laid out in Roskam [9]. The x-plot is shown in Figure 5.10. A constraint of 4.0% was placed on the minimum tolerable static margin for piloting, and the smallest planform area of 1.0 ft^2 was selected for this margin. The longitudinal stability derivatives were then calculated for the range of stabilator spans and chords that maintained this surface area. Trim diagrams were produced for each possibility, establishing the flight envelope between the forward and aft center of gravity limits and the stall angle. If at least 10% of the control authority was outside the flight envelope, it was determined to be sufficiently able to maneuver out of the trimmed condition. The necessary deflection angle for trimmed C_{Lmax} was then calculated and minimized by the span and chord pairing for the horizontal tail. The trim diagrams are given in Figure 5.11 for the chosen tail size of 0.5’ chord and 2.0’ span.

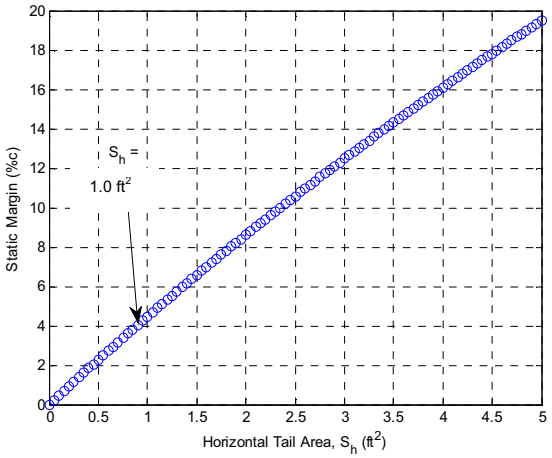

Figure 5.10: Longitudinal Stability X-Plot

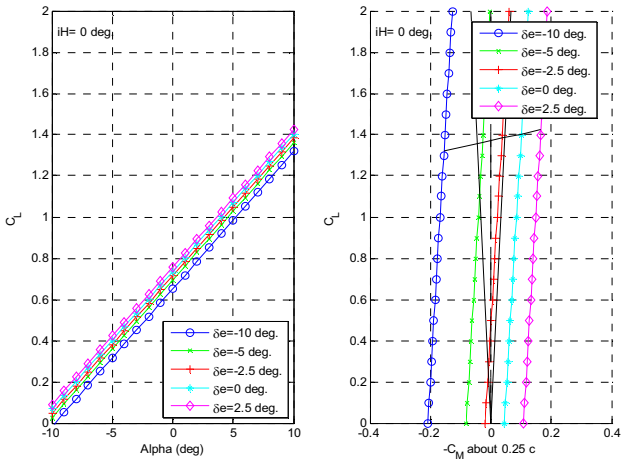

Figure 5.11: Aircraft Trim Diagram

5.3.2 Directional Stability and Control

The vertical tail area was determined through the directional stability coefficients. Similar to the horizontal tail, a directional stability x-plot was created to establish the vertical tail size as a function of the yawing moment coefficient due to sideslip, $C_{n,\beta}$. The smallest vertical tail area of 0.667 ft^2 providing a positive $C_{n,\beta}$ was chosen, as shown in Figure 5.12. A MATLAB Simulink simulation of the arbitrary motion of the aircraft allowing for six degrees of freedom was used to analyze the stability of the aircraft. The solutions to the differential equations were obtained through two methods: numerical integration through Simulink and linearization to obtain the approximate solution. This simulation assumed a flat earth and rigid body dynamics. The input consisted of 67 constants given from the geometric parameters and flight conditions. Empirical tables are then used to predict the 21 stability and control derivatives[10]. Control surface deflection, horsepower, and wind gust perturbations can also be entered into the simulation. This simulation was used to determine the necessary size of the rudder to dampen out the effects of a 10 ft/s wind gust within 3 seconds. The resulting rudder encompassed the entire span of the vertical tail and half of the chord. Shown in Figure 5.13 is the aircraft's response over time to a 10 ft/s wind that begins at t=10 seconds.

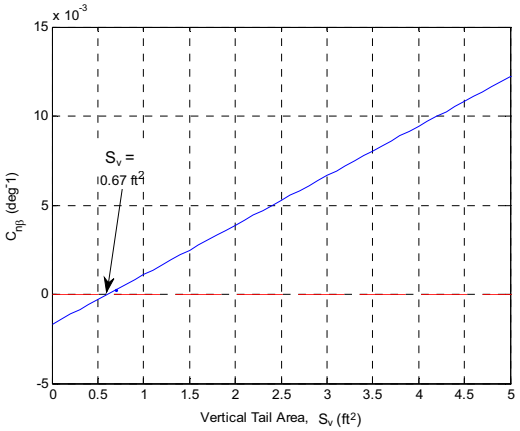

Figure 5.12: Directional Stability X-Plot

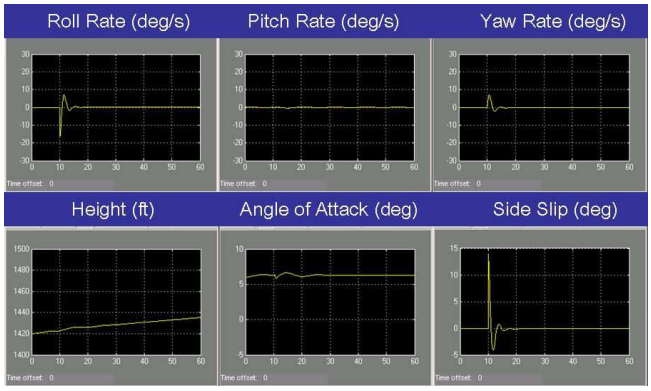

Figure 5.13: Aircraft Response to 10 ft/s Wind at t=10s

5.3.3 Lateral Control

The ailerons were sized to reach the required bank angle of 30° (determined during aircraft sizing) within one second. This analysis was done in a similar fashion to the rudder sizing with 15° of aileron deflection. With a 3" chord and 10.5" span for each aileron, the desired bank angle is reached in 0.47 sec.

5.3.4 Flap Sizing

The addition of flaps inboard of the ailerons increases the aircraft's lift during takeoff, where the propulsion requirement is the greatest. This reduces the thrust constraint on takeoff and allows for a smaller, lighter propulsion system, and thus a higher score. A 30% wing chord length was chosen for compatibility with the spar location determined by the ailerons. The flaps span 67% of the wing, using all of the available span inboard of the ailerons. The slotted flap design gives the highest additional lift and lowest drag relative to plain and split flaps, and is relatively easy to manufacture. These flaps achieve maximum lift at a 40° deflection angle, resulting in an increase of C_{Lmax} of 1.05 [11]. The profile drag coefficient is raised by 0.12, while the angle of attack for maximum lift is reduced by 2°.

5.3.5 Control Surface Sizes

The control surface sizes determined in the stability and control analysis for the BoilerBus2 aircraft are provided in Table 5.2.

Table 5.2: Control Surface Sizes

Control Surface	Stabilator	Rudder	Ailerons (each)	Flaps (each)
Chord (ft)	0.50	0.40	0.30	.19
Span (ft)	1.80	1.00	0.88	1.68

5.4 Structures

Detailed design of the aircraft structure focused primarily on the internal wing design. In particular, designs are evaluated on the basis of estimated weight by evaluating bending capacity before failure and

deflection at maximum loading conditions. Two concepts selected for evaluation from preliminary design included a conventional rib/spar wing and a hollow shell composite wing, as shown below in Figure 5.14.

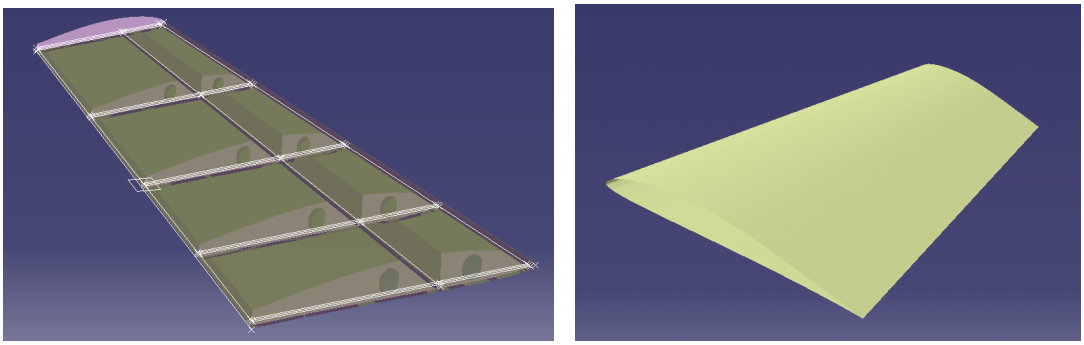

Figure 5.14: Conventional and Hollow Wing Design

5.4.1 Hollow Wing Analysis

The choice of composite materials was limited by material availability and ease of manufacturing, with the thinnest workable balsa found to be .0312" (Orchoma Pro-Balsa) and the thinnest fiber glass to be 0.004" dry (S-Glass Fiber/Epoxy 65-70% Polymer). A balsa shell by itself would be structurally inadequate and extremely prone to cracking without reinforcement. Thus, a top layer of glass fibers of +45/-45^{o} orientation for increased torsional rigidity and fracture prevention was required. Due to the inherent complexity of the laminate material properties [12], an analytical MATLAB algorithm combining Simple Beam Theory with Classic Laminate Theory was validated using a linear span-wise load distribution and used in lieu of a finite element method (FEM). Polar moment of inertia for 3D wing geometry of the BoilerBus2 aircraft was computed using thin walled closed cell theory. The wing was then modeled as a cantilever beam with the hollow space simulated by a zero stiffness core. Although the laminate/balsa sheet was not symmetric, the inclusion of the hollow core section made the overall laminate symmetric, as seen in Figure 5.15. This approach eliminates flexural-extension coupling.

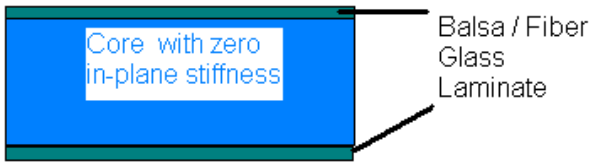

Figure 5.15: Final Analysis Laminate

For this analysis, the wing deflection in bending, twist, and maximum stress were the only values of interest. Thus, the root cross-section was chosen as the discrete location for which to evaluate the hollow wing laminate thickness used in bending analysis. The average thickness of the root airfoil was found to be 2.75", and the maximum thickness of the top plate was 2.13". The resulting wing tip twist calculated changed linearly from 0^{o} to 0.5^{o} for 0 to 120 in-lbs of applied torque respectively. The conclusion was

negligible tip twist and an acceptable overall maximum tip displacement of 0.12” over the full range of applied torques. The bending stress experienced by each section of laminate (balsa and fiberglass) was well within the failure tolerances of each material.

5.4.2 Conventional Wing Analysis

The conventional balsa rib and spar design consisted of a single sheet layer of .0312” thick balsa as skin. Since this design does not include laminates, it was analyzed in the ANSYS FEM package using an Excel input file. The number of ribs and spars were variables, with at least two main spars required for torsional rigidity. Optimal loading conditions favored a continuous main spar running from wing tip to wing tip. Wing incidence affected the orientation of the main spar since it must remain parallel to the payload bay dividers in the aircraft fuselage. The spar thicknesses were set to 0.25” and the ribs to 0.0675” based on previous year’s designs. All members were assumed to be isotropic for simplicity. The longitudinal Young’s modulus was used instead of the transverse Young’s modulus assuming that the balsa is aligned such that its grain (the stiffer direction) would take the bulk of the loading.

Actual wing loads from CFD analysis in FLUENT at 15^{o} angle of attack during cruise was used in this validation. The static pressure distribution was averaged over three chord-wise main sections of the wing. The resulting non-linear pressure distribution simulated the unbalanced flight loads that generate wing twist. The results of the analysis, as shown in Figure 5.16, indicated tip displacement due to non-linear loading to be on the order of 0.04”. The experienced stresses were within tolerances of the material and were later found to be similar in concentration to the linear loading case.

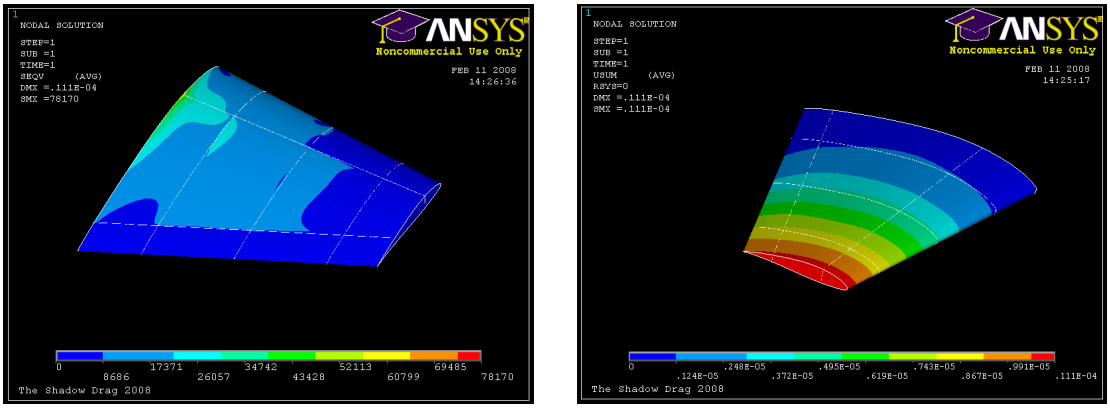

Figure 5.16: Wing Loading Stress Distribution Validation

Since model validation showed that non-linear chord wise pressure distribution could be ignored, an equally distributed load was conservatively based on a 14 lbf aircraft at 2.5g wing loading (same magnitude of the load as that used in the hollow wing analysis). The number of ribs was estimated at 5, and the aft spar was held fixed due to control surface size constraints. Figure 5.17 shows maximum stress at the main spar root for different chord-wise placements of the forward spar. The maximum stress occurred at the top of the main spar root in each case.

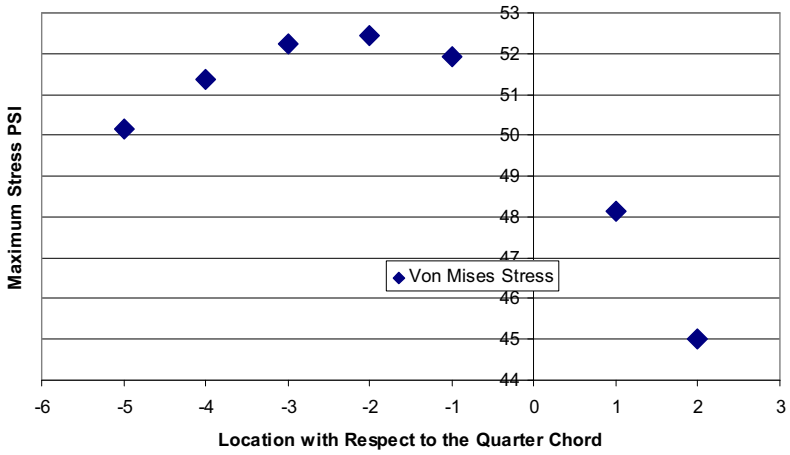

Figure 5.17: Maximum Compressive Stresses in Wing/von Mises Dependency on Main Spar Location

From Figure 5.17, we see that the ranges of maximum stresses in the wing are well within material tolerances. Moving the spar forward of the quarter chord resulted in the most significant stress reduction. Furthermore, at one inch in front of the quarter chord, the main spar can pass freely through the fuselage. Thus, one inch in front of the quarter chord was chosen as the optimal location for the main spar. It was also noted that although the maximum thickness of the wing cross-section occurs a few inches aft of the quarter chord, forward main spar placement allowed for greater load distribution to the aft spar resulting in overall lower maximum stress concentration.

5.4.3 Comparison and Analysis Conclusions

Both wing designs proved capable of handling the loads under a 2.5g, 14 lbf aircraft flight condition. The stress experienced by the hollow wing was two orders of magnitude greater than that of the conventional wing but still within material tolerances. Hence, weight was the deciding factor as shown in Table 5.3.

Table 5.3: Weight Estimates for Conventional and Hollow Wing Designs

	Conventional Design	Hollow Wing Design
Weight Fraction: Balsa Skin	0.5	0.35
Weight Fraction: Balsa Internal	0.5	0
Weight Fraction: FG/Epoxy	0	0.65
Total Weight (lbf)	1	1.44

The hollow wing was estimated to be 0.44 lb heavier than the conventional design primarily due to the weight of epoxy resin used in curing the composite. Therefore, based on the above weight comparison, the conventional wing design was chosen.

For additional weight reduction on the conventional design, several main spar designs were considered, as shown in Figure 5.18. Since the orthotropic properties of balsa prevent stiffness in both directions, two

balsa plates with one side orientated for shear loading and the other for axial loading was favorable. Design D was chosen since it allowed for adhesion of the spar to the main wing.

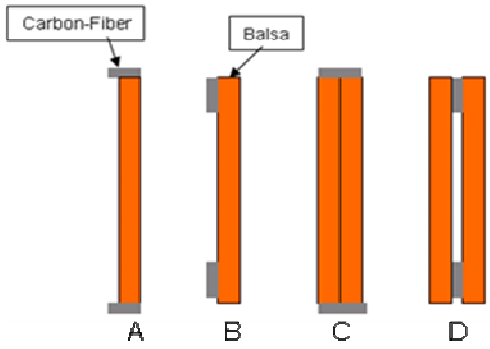

Figure 5.18: Main Spar Construction Designs

FEM analysis on the chosen spar configuration allowed for different thicknesses of balsa wood to be evaluated. The spar was clamped in the fuselage by two balsa plates and a linearly distributed span-wise load was applied along the length of the spar. A 2.5g distributed force for a 14 lbf aircraft was applied to the bottom surface. Analysis results shown in Figure 5.19 reveal that 0.0312" x 0.128" carbon fiber strips and 0.0312" balsa sides withstood the entire bending load of the wing with negligible displacement. The bending stress peaks at 1.47×10^8 Pa in the carbon fiber strip with maximum tip displacement of 0.21".

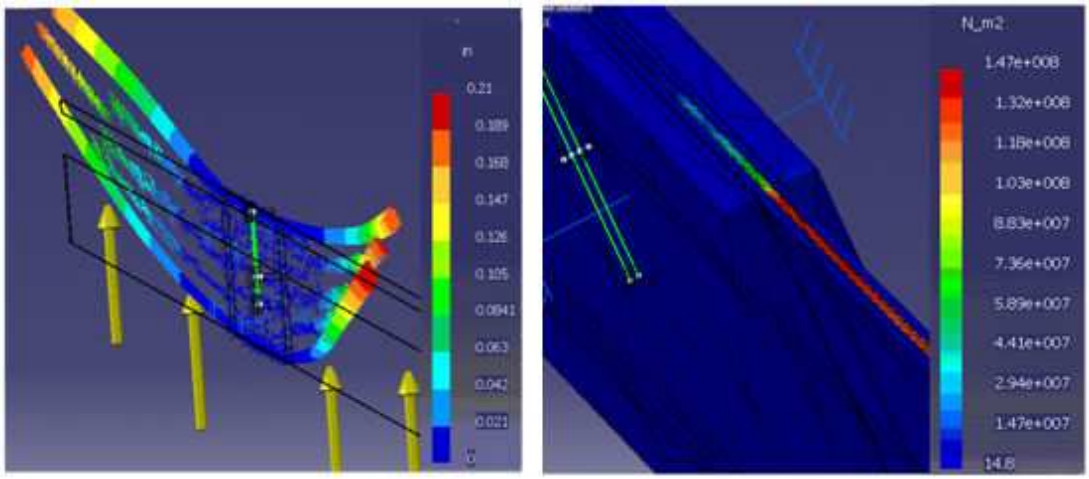

Figure 5.19: Stress Distribution and Displacement of Wing: 0312" Balsa and Carbon Fiber

The maximum stresses in both the balsa wood and the carbon fiber are within tolerance and an order of magnitude away from failure. The displacement field indicates not only vertical displacement, but axial twisting due to the orthotropic nature of the balsa wood. In Figure 5.19, two 0.125" balsa wood strips were used, however, the strip on the left most side had its grain aligned with the length of the wing while the strip on the right most side had its grain orientated vertically. This phenomenon can be used advantageously by having the main spar twist against the aerodynamic twisting of the wing.

The main spar will take the majority of the bending while the aft and main spars combined will handle the torsional loading. Since the main spar is constrained to being overbuilt by the scale of the materials, the 0.0312” thick balsa skin on the wing could be replaced with lighter materials such as MonoKote. The only restraining factor comes from maintaining sufficient torsional resistance and the ability of the skin to maintain its shape. This leaves the possibility of adopting a hybrid skin construction, one which resembles the BiolerBus1’s skin, which has the leading edge skin made of balsa and the trailing half of the wing’s skin made of MonoKote.

5.5 Propulsion

Aircraft propulsion selection requires consideration of several components: motor, battery, gear box, and propeller. Initially, each part was individually analyzed; however, it soon became clear that each system was closely related to the other, complicating the analysis. Battery voltage and current draw dictate the RPM of the motor, the RPM of the motor/gearbox dictates the current drawn by the propeller, and the current drawn by the propeller alters the voltage of the battery. In order to efficiently determine the best propulsion system configuration, a computer program that iterated through all available motors, batteries, propellers, and gear boxes that fell in the range of aircraft and mission specifications was required. To determine the propulsion system properties, electric motor theory and propeller wind tunnel data was used to create two new computer programs. One program determines the motor parameters given a thrust required, which is used for the cruise and turn portions of the mission. The other program determines the maximum possible thrust of the motor system, which is used for takeoff. A flow chart representing these computer programs as well as their basic equations are shown in Figure 5.20.

Both computer programs require the motor constants (RPM/Volt, no load current, and resistance), battery parameters (voltage output as a function of current), and propeller parameters (coefficient of power and coefficient of thrust curves). The motor and battery data was determined from manufacturer’s specifications. Data on the propellers was not available, so a database of these specifications was created through wind tunnel testing, as summarized in Section 8.1.1.

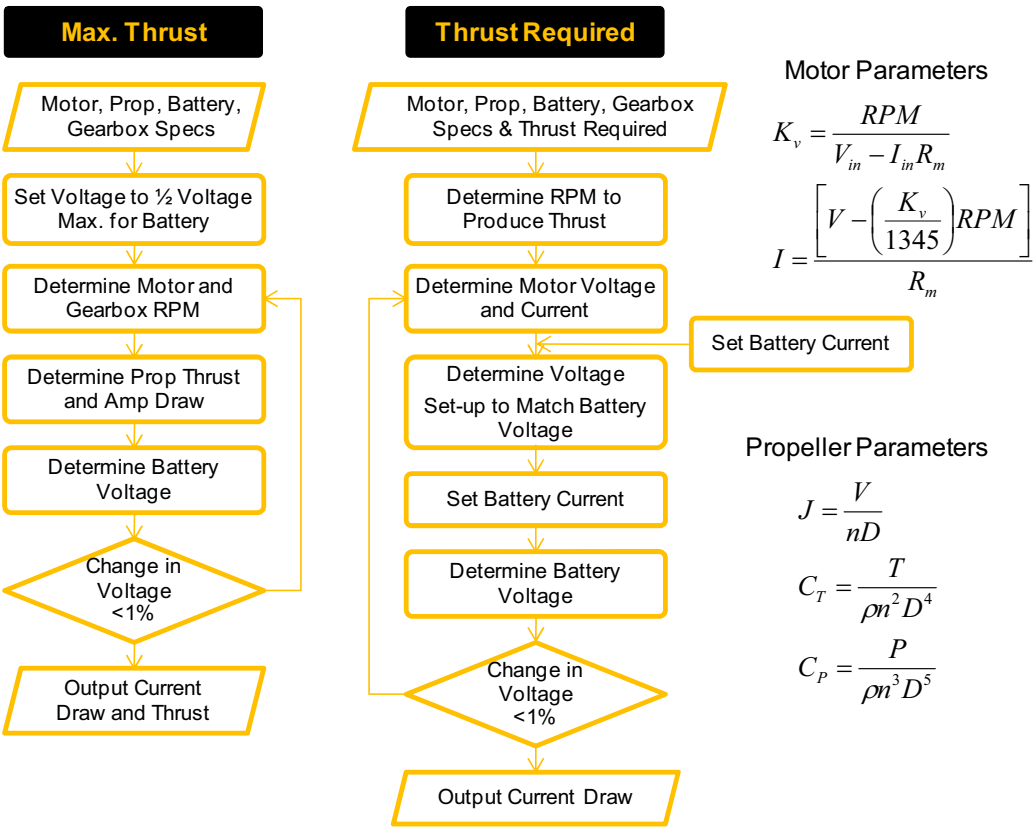

Figure 5.20: Propulsion Code Program Flow Charts

Once these analysis programs were created, an additional program was created to loop through all the possible combinations of propellers, gear boxes, motors, batteries, and number of cells. The program went through each combination to determine if the system met the take-off distance, thrust requirements for the cruise and turn portions of the mission flight profile, and sufficient battery energy to complete the mission. Finally, the computer program took into consideration that a pilot of a radio-controlled airplane would not be able to fly the plane at the exact optimal points. To counterbalance the human error, a 20% safety factor was added to the battery energy required. Every combination that met the requirements was saved and a mission score calculated. The scores were then sorted and the best motor configurations were identified.

Large current draws are required in order to meet the 75' takeoff distance requirement for Mission 2, but due to the short mission duration only a small amount of battery is required. The voltage of the batteries is highly dependant on the current draw, as shown in Figure 5.21. Once the current reaches twenty times the capacity of the battery, the voltage begins to drop rapidly. Results from the propulsion analysis reveal that the batteries are not able to meet the voltage needed by the motor to match the RPM required by the propeller to produce the proper amount of thrust. As a result, there is a point at which decreasing the aircraft's size to minimize power required for flight is outweighed by a larger battery needed to meet the voltage requirements of takeoff. In order to determine this point, several different aircraft sizes that had

been studied by the initial sizing analysis were run through the propulsion system analysis. The results are shown in Figure 5.22.

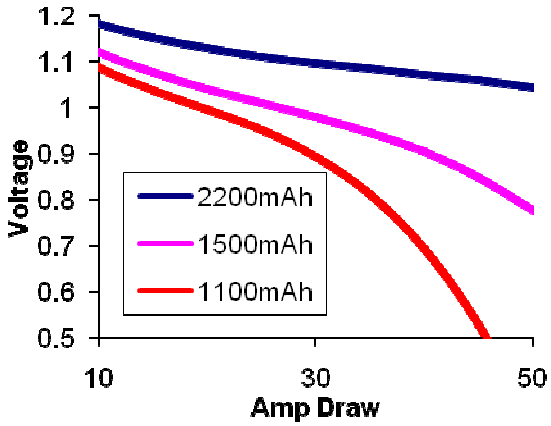

Figure 5.21: Voltage vs Amp Draw

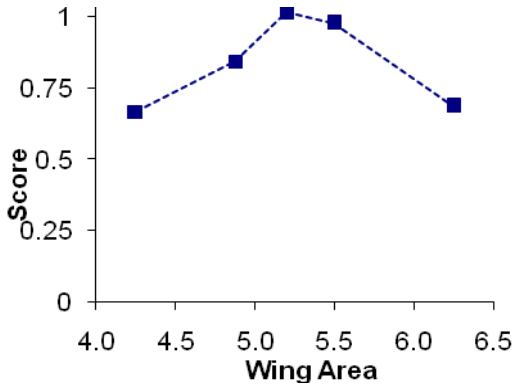

Figure 5.22: Mission 2 Score Comparison

The propulsion system trade study verified that the chosen wing area of approximately 5.2 ft^2 yielded the highest score and was just above the limit, approximately 4.9 ft^2, where the battery required to meet takeoff voltage outweighs the battery required for flight. From this point, the analysis was conducted for the exact mission specifications and the chosen aircraft to determine the combination of motor, gear box, battery, number of battery cells, and propeller that yielded the highest score for each mission. The configurations studied are summarized in Table 5.4 and the results for the top combinations and their scores are provided in Table 5.5. Over 200,000 different combinations were analyzed and the scores were normalized to the best scores for Mission 1 and Mission 2. The motor finally chosen was the Neu 1107-2Y (3400 RPM/Volt) with a 6.7:1 planetary gearbox. The motor was paired with an 18” x 10” APC propeller and 9 Elite 1500 batteries. The system produces 91 oz. of static thrust and requires 450 watts. The selected propulsion system was also chosen because in several different configurations it ranked top in score. Thus, if a design change is required (such as an increased thrust requirement) the system would still rank highly.

Table 5.4: Available Configurations

Gearboxes	
Type	Gear Ratios
None	1 to 1
Neu Box Planetary	3.7,4.4,5.3,6.7 to 1
Hacker Small Planetary	4 to 1
Hacker Large Planetary	3.7,5.2,6.7 to 1
Kontronik Planetary	3.7,4.2,5.2 to 1

Batteries
Gold Peak GP2200
Elite 1500
Gold Peak GP1100
Kan 700

Propellers (data from wind tunnel Tests)	
Diameter (in.)	Pitch (in.)
14	8,10,12
16	8,10,12
18	10,12
20	8,10

Brushless Motor Types (# Studied)
Axi Out-runners (12)
Neu In-runners (27)
Hacker In-runners and out-runners (151)
Kontronik In-runners (4)
Plettenburg In-runners (3)

Table 5.5: Top Scoring Configurations

		Mission 2				Mission 1				
Motor #	Gear Ratio	Battery	Number of Cells	Prop Diameter (in.)	M2 Score	Battery	Number of Cells	Prop Diameter (in.)	M1 Score	Total Score
Neu 1107-2Y	6.7	Elite 1500	9	18x10	100.0	Kan 700	4	18x10	50.0	150.0
Neu 1110-1.5Y	6.7	Elite 1500	9	18x10	99.2	Kan 700	4	18x10	50.0	149.2
Neu 1110-2Y	4.4	Elite 1500	9	18x10	99.2	Kan 700	4	18x10	50.0	149.2
Hacker B50 10S	6.7	Elite 1500	9	18x10	94.9	Kan 700	4	18x10	50.0	144.9
Hacker B50 13S	5.2	Elite 1500	9	18x10	94.8	Kan 700	4	18x10	50.0	144.8

5.6 Flight Mission Performance and RAC

Dimensional parameters and mission profile predictions for the final competition aircraft are summarized in Table 5.6.

Table 5.6: Aircraft and Mission Characteristics

RAC	
RAC Mission 1	0.447
RAC Mission 2	1.578
Geometry	
Wings	
Airfoil	Eppler 210
Mean Chord (in)	14.70
Span (in)	60.00
Area (ft^2)	5.20
Taper Ratio	0.45
AR	4.81
Stabilator	
Airfoil	NACA 0008
Chord (in)	6.00
Span (in)	24.00
Area (ft^2)	1.00
AR	4.00
Vertical Tail	
Airfoil	NACA 0008
Chord (in)	8.00
Span (in)	12.00
Area (ft^2)	0.67
AR	1.49
Fuselage	
Length (in)	48.00
Width (in)	9.25
Height (in)	8.75

Performance (Predicted)	
C_L max (w/flaps)	2.474
L/D max	6.300

Gross Weight Performance (Predicted)		
	Mission 1	Mission 2
(Rate of Climb) max (ft/min)	200	300
Stall Speed (ft/s)	15	26
Flight Velocity (ft/s)	21	41
Take Off Distance (ft)	24	75
Weight		
	Mission 1	Mission 2
Motor (lb)	0.20	0.20
Propeller (lb)	0.14	0.14
Airframe (lb)	2.57	1.85
Gearbox (lb)	0.14	0.14
ESC (lb)	0.06	0.06
Avionics (lb)	0.23	0.23
Servos (lb)	0.30	0.30
System Weight (lb)	3.65	2.92
Batteries (lb)	0.12	0.54
Payload Weight (lb)	0.00	7.00
Gross Takeoff Weight (lb)	3.65	10.46
Systems		
	Mission 1	Mission 2
Propeller	APC 18x10E	APC 18x10E
Batteries	4 Kan 700 AA	9 Elite 1500
Servos	6 Futaba S3150	
Gearbox	Neu Box 15 Series 6.7:1 gear ratio	
Reciever	Berg 7P	
RX battery	Hobbico 4.8V 1200 mAh NiMH Flat	
ESC	Castle Creations Phoneix 45	
Motor	Neu 1107-2Y	

The table of all of the major components of the aircraft was made to determine the center of gravity and moments of inertia of the aircraft. This took into account batteries, motors, servos, frame, control surfaces, and skin weights and location. The location is based off of an XYZ coordinate system centered at the nose of the aircraft. X is the roll axis, Y is the pitch axis, and Z is the yaw axis, with Z pointing in the up direction. A CAD model in CATIA was used to find the CG of the fixed components, such as the airframe and motors. The location of the batteries was allowed to be movable to balance the aircraft's CG. The CG of the aircraft was calculated assuming point masses. The moments of inertia were calculated using the same methods as the CG. Figure 5.23 shows the CG for the aircraft and the local CG of the major components.

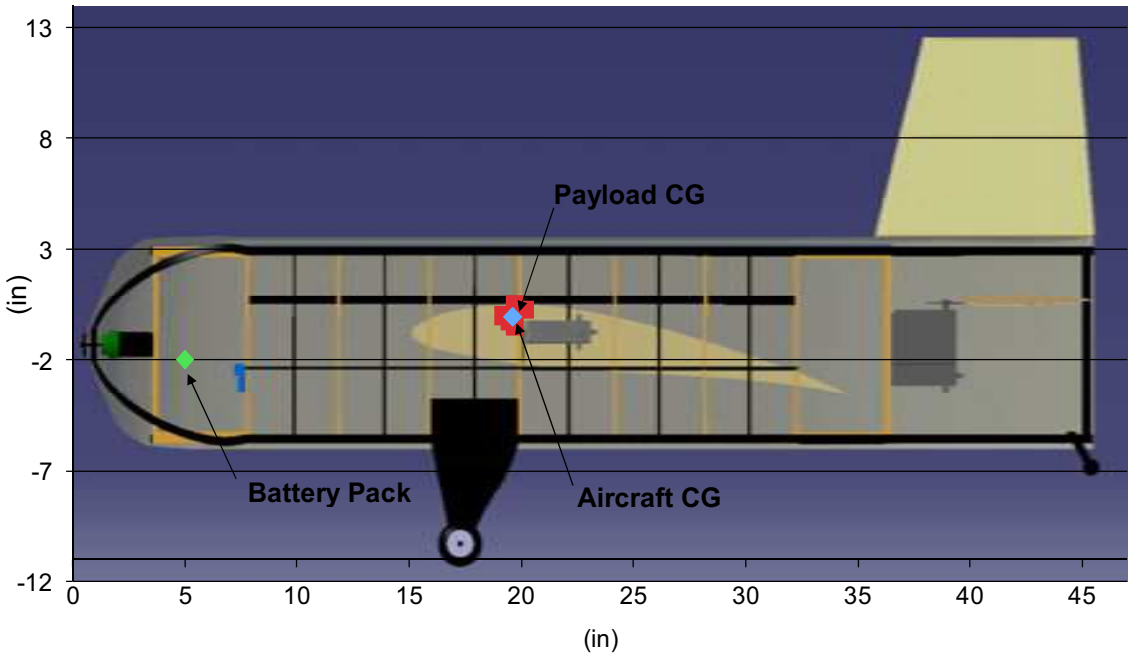

Figure 5.23: Aircraft CG and Component CG Locations

Tables 5.7 and 5.8 summarize the aircraft CG and aircraft weight and moments of inertia for each payload combination.

Table 5.7: Aircraft CG Locations

	CG (Predicted		
	X (ft)	Y (ft)	Z (ft)
Combo 1	1.64	0	-0.04
Combo 2	1.64	0	0.01
Combo 3	1.62	-0.01	-0.03
Combo 4	1.61	0	-0.02
Combo 5	1.66	0	0
No	1.61	0	-0.05

Table 5.8: Aircraft Weight and Moments of Inertia

	A/C weight	Moments of Inertia (lb ft^2)					
	Weight (lbf)	Ixx	Iyy	Izz	Ixy	Ixz	Iyz
Combo 1	10.82	1.02	31.904	32.642	0.085	-0.757	-0.006
Combo 2	11.02	1.02	32.444	33.181	0.085	0.214	-0.006
Combo 3	10.62	1.011	30.912	31.659	0.085	-0.508	-0.006
Combo 4	10.92	1.008	31.24	31.99	0.085	-0.279	-0.006
Combo 5	10.72	1.011	32.446	33.193	0.085	-0.038	-0.006
No	3.4	0.996	10.721	11.459	0.014	-0.184	-0.006

5.7 Computer Aided Design (CAD)

5.7.1 Design Approach

CATIA was chosen as the main CAD package for constructing models and components. A novel method was introduced taking CATIA's ability to use design tables, allowing parameters used in CATIA to be mapped into an external file and vice versa. Microsoft Excel spreadsheets were created which were linked to dummy points in CATIA. The position of these dummy points can be driven by simply changing parameters in the spreadsheets. The data points were then connected by automatically updating the geometry in CATIA. Figure 5.24 (a) shows a sample of the design table used in Excel. For example, wing design parameters have wing span, taper ratio, chord, etc., as variables. Figure 5.24 (b) also shows the corresponding data points and splines (for the wing only) in CATIA (other aspects of the model are hidden here). Figure 5.24 (c) shows the final surface lofted over the splines. Initial fuselage designs were driven by the payload configuration and aircraft size constraint given by the mission requirements, resulting in an 8" x 8" x 28" rectangular box. The forward and aft closure of the fuselage was driven by aerodynamic performance. Wings and control surfaces were generated by data points from the UIUC airfoil database [13] text files and then linked to parameters in the design table. The entire aircraft was then readily updated and modified through an interface similar to that shown in Figure 5.24.

Design Parameters in British (fps) and mks Units				
		in	ft	meters
Wing Design Parameters				
Wing Span			2.50	0.76
Taper Ratio	0.45			
Wing Root Chord		19.47	1.62	0.49
Wing Tip Chord		8.76	0.73	0.22
Wing Location		13.80	1.15	0.35
Dihedral (deg)	4.00			
Sweep (deg)	30.00			
Twist				
Number of Airfoils	18.00			
Horizontal Tail Design Parameters				
HT Span			0.75	0.23
Taper Ratio	0.50			
HT Root Chord			0.35	0.11
HT Tip Chord			0.17	0.05
HT Location (m)		40.00	3.33	1.02
HT Height			0.00	0.00
Dihedral (deg)	3.00			
Sweep (deg)	0.00			
Twist				0.00
HT Height				
Vertical Tail Design Parameters				
VT Height			1.00	0.30
Taper Ratio				
VT Root Chord			0.42	0.13
VT Tip Chord			0.00	0.00
VT Location (m)		40.00	3.33	1.02
Sweep (deg)	10.00			
Twist				
Fuselage Parameters Design Parameters				

(a)

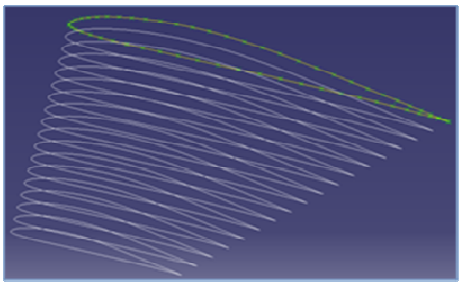

Point and Spline Construction of Wing Geometry

(b)

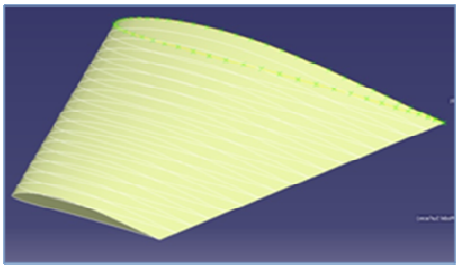

Final Surface Geometry for a Wing Structure

(c)

Figure 5.24: Design Table and Generated Model

5.8 Drawing Package

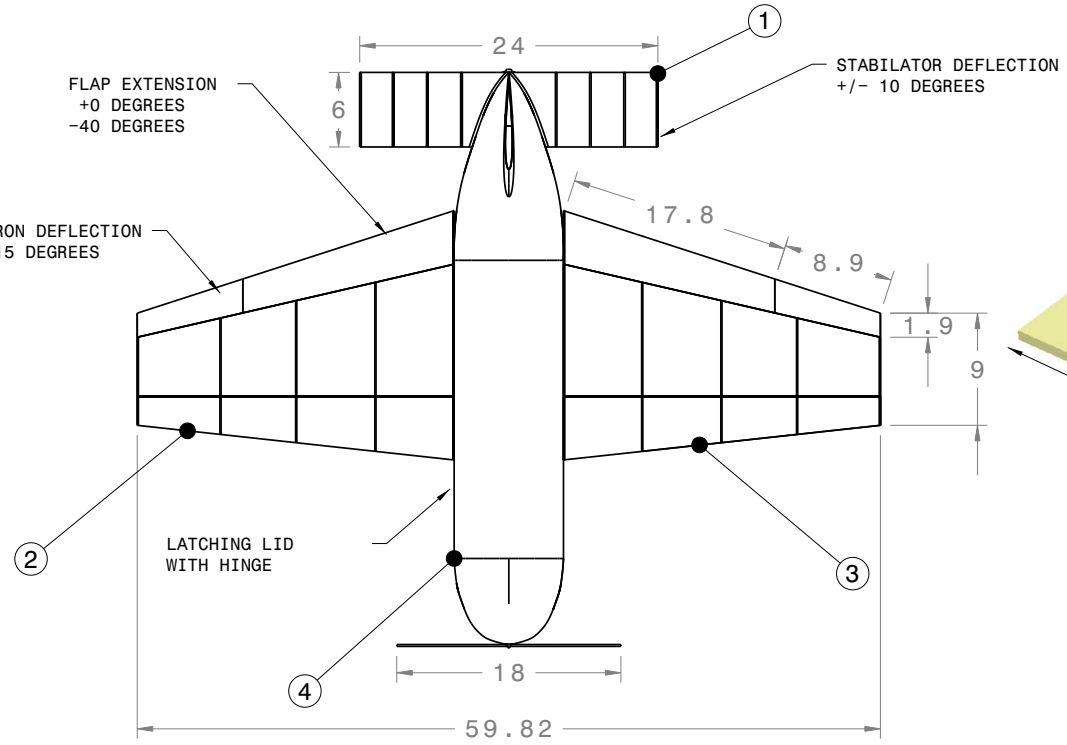

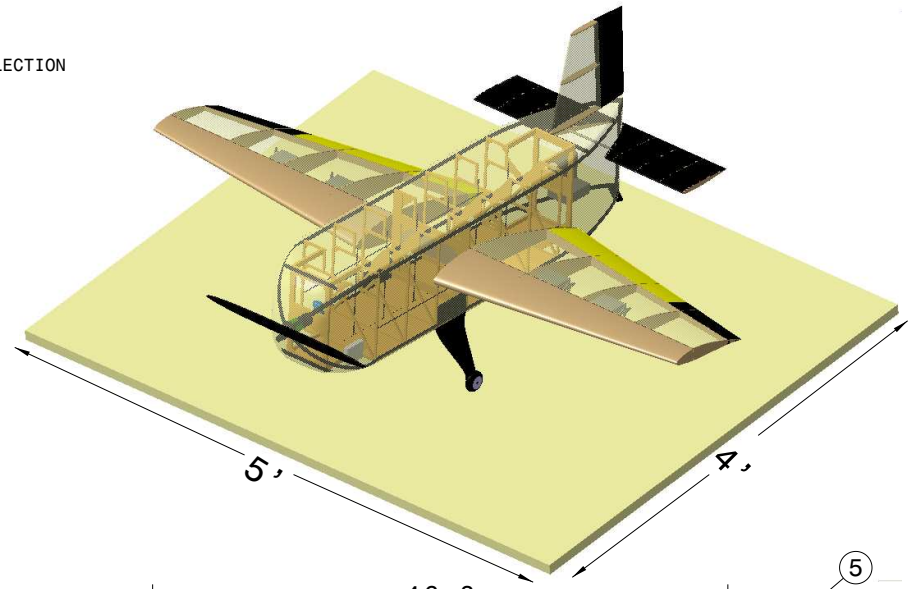

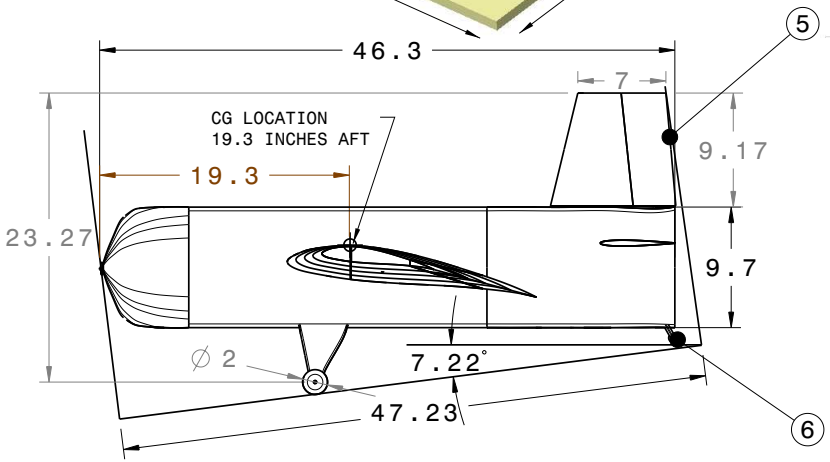

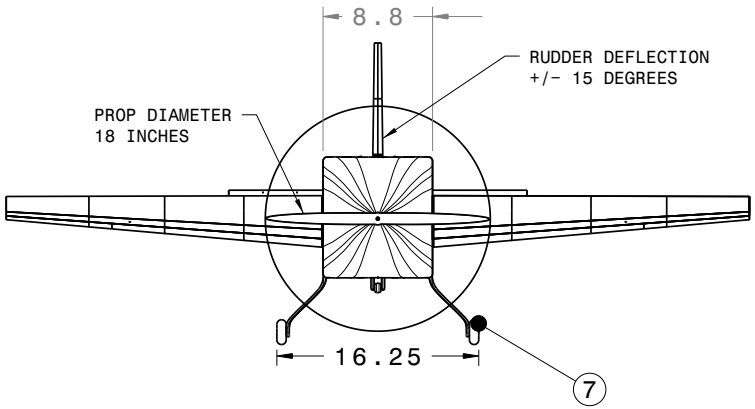

	PRIMARY COMPONENTS
1	HORIZONTAL TAIL ASSEMBLY
2	RIGHT WING ASSEMBLY
3	LEFT WING ASSEMBLY
4	FUSELAGE
5	VERTICAL TAIL ASSEMBLY
6	TAIL LANDING GEAR
7	MAIN LANDING GEAR

NOTE: ALL DIMENSIONS ARE GIVEN IN INCHES

PURDUE UNIVERSITY TEAM SHADOW DRAG
AIAA DBF 2008

3-VIEW

SCALE: 1:10 | 2-27-2008

DRAWING PACKAGE | PAGE 1 OF 4

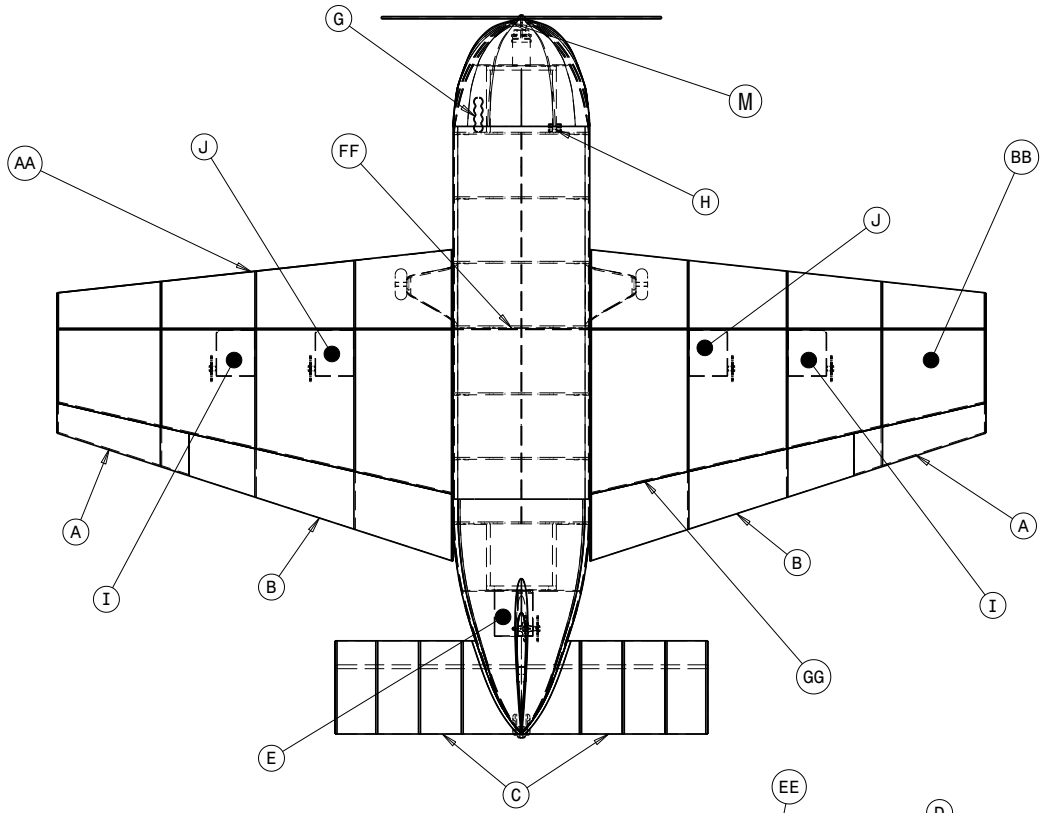

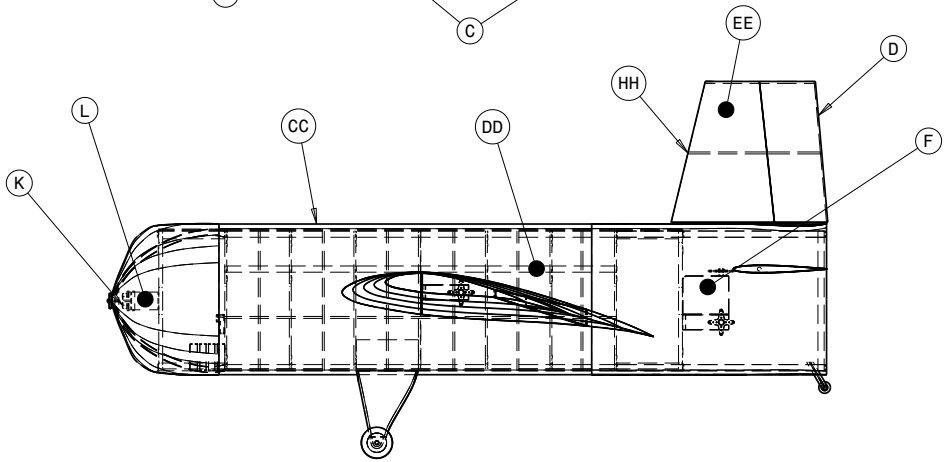

CONTROL SYSTEM COMPONENTS

	DESCRIPTION	MATERIAL
A	AILERON	BALSA/ MONOKOTE
B	FLAP	BALSA/ MONOKOTE
C	STABILATOR	BALSA/ MONOKOTE
D	RUDDER	BALSA/ MONOKOTE
E	STABILATOR SERVO	FUTABA S3150
F	RUDDER SERVO	FUTABA S3150
G	PROPULSION BATTERY	9x ELITE 1500 / 4x Kan 700
H	RECEIVER	BERG 7
I	AILERON SERVO	FUTABA S3150
J	FLAP SERVO	FUTABA S3150
K	MOTOR	NEU 1107 2Y
L	GEAR BOX	NEU BOX 15XX
M	SPEED CONTROLLER	C.C. PHOENIX 45

STRUCTURAL COMPONENTS

	DESCRIPTION	MATERIAL
AA	WING RIB	BALSA
BB	WING SKIN	MONOKOTE
CC	FUSELAGE SKIN	MONOKOTE
DD	INTERNAL STRUCTURE	CARBON
EE	VERTICAL TAIL SKIN	MONOKOTE
FF	MAIN WING SPAR	BALSA/ CARBON
GG	AFT WING SPAR	BALSA
HH	VERTICAL TAIL RIB	BALSA
II	PAYLOAD STRUCTURE	BALSA

BOILER BUS

NOTE: ALL DIMENSIONS ARE GIVEN IN INCHES

PURDUE UNIVERSITY TEAM SHADOW DRAG
AIAA DBF 2008

SYSTEMS LAYOUT

SCALE 1:8 | 2-27-2008

DRAWING PACKAGE | PAGE 4 OF 4

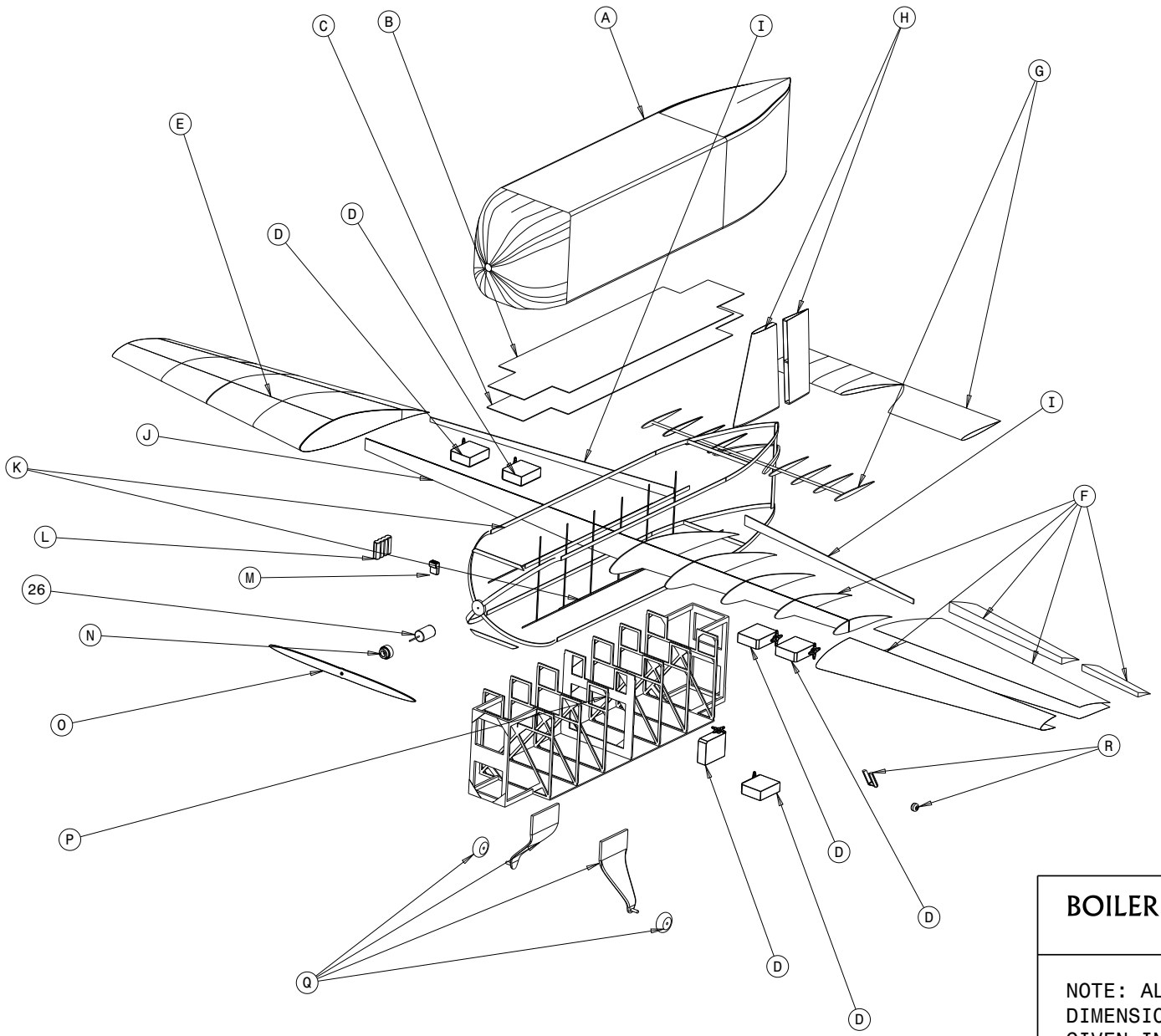

	COMPONENT	MATERIAL
A	FUSELAGE	COMPOSITE
B	PAYLOAD HATCH	BALSA
C	PAYLOAD RESTRAINT	BALSA
D	SERVO	FUTABA S3150
E	RIGHT WING ASSEMBLY	BALSA/FIBERGLASS/ COMPOSITE
F	LEFT WING ASSEMBLY	BALSA/FIBERGLASS/ COMPOSITE
G	HORIZONTAL TAIL ASSEMBLY	BALSA/COMPOSITE
H	VERTICAL TAIL ASSEMBLY	BALSA/COMPOSITE
I	AFT SPAR	BALSA/CARBON
J	MAIN SPAR	BALSA/CARBON
K	INTERNAL STRUCTURE ASSEMBLY	CARBON
L	BATTERY PACK	HOBBICO 4.8V
M	RECEIVER	BERG 7
N	GEAR BOX	NEU BOX 15XX
O	PROPELLER	APC 18 INCH
P	PAYLOAD SUPPORT ASSEMBLY	BALSA
Q	MAIN GEAR ASSEMBLY	BALSA/CARBON FIBER
R	TAIL GEAR ASSEMBLY	BALSA/CARBON FIBER
S	MOTOR	NEU 1107 2Y

BOILER BUS

NOTE: ALL DIMENSIONS ARE GIVEN IN INCHES

PURDUE UNIVERSITY TEAM SHADOW DRAG
AIAA DBF 2008

STRUCTURAL ARRANGEMENT

SCALE 1:10 | 2-27-2008

DRAWING PACKAGE | PAGE 3 OF 4

PAYLOAD 1 - 4 BRICKS

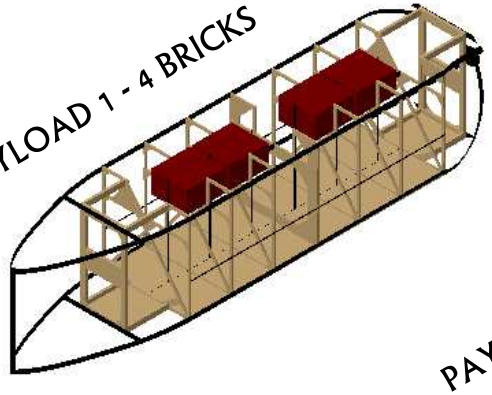

PAYLOAD 2 - 2 BRICKS, 7 BOTTLES

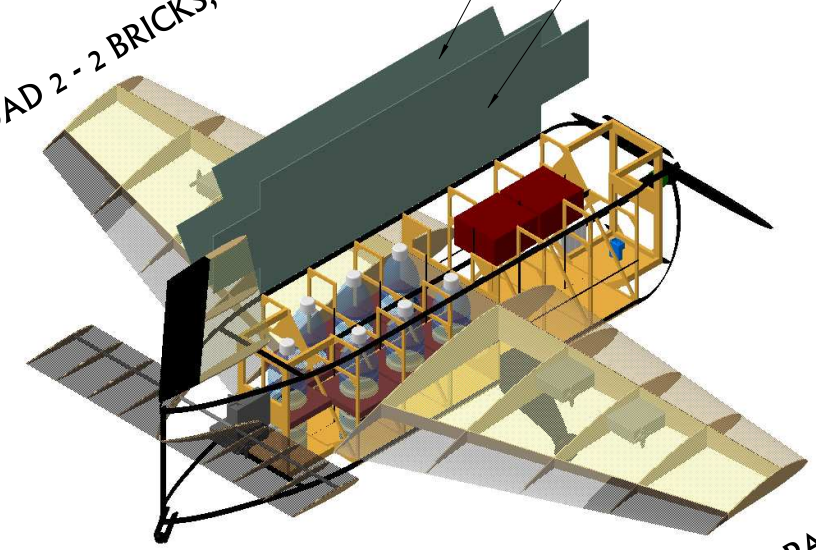

PAYLOAD 3 - 14 BOTTLES

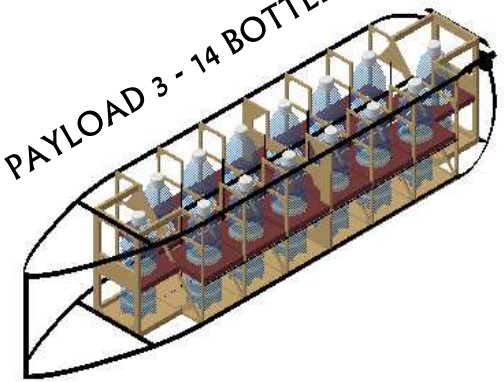

PAYLOAD 4 - 3 BRICKS, 3 BOTTLES

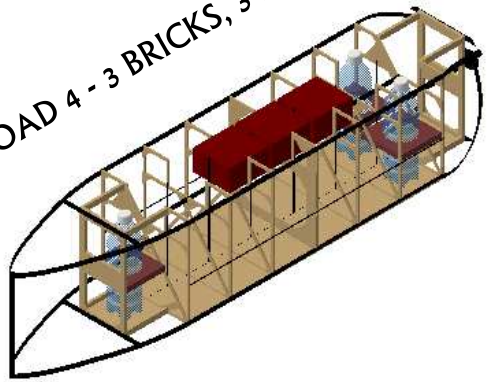

PAYLOAD 5 - 1 BRICK, 10 BOTTLES

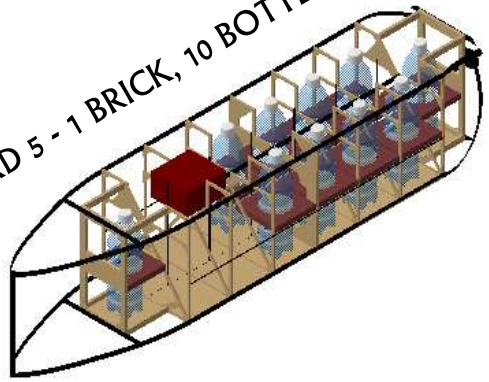

BOILER BUS	PURDUE UNIVERSITY TEAM SHADOW DRAG AIAA DBF 2008
NOTE: ALL DIMENSIONS ARE GIVEN IN INCHES	PAYLOADS ACCOMMODATION
	2-27-2008
	DRAWING PACKAGE — PAGE 2 OF 4

6 MANUFACTURING

6.1 Manufacturing Processes

The manufacturing processes used in the construction of the final design, BoilerBus2, were an assortment of conventional model aircraft construction techniques and newer techniques using composite materials in an effort to produce the lightest airframe possible. The selection of construction processes and methods took a number of factors into account, including availability of materials, the construction abilities of the team, ease of repair, and weight. Construction methods of previously successful competition teams were investigated and in some cases implemented to determine the best processes that result in the lightest airframe. Techniques and materials investigated included foam construction, balsa/fiberglass laminates, carbon-fiber rods and cloth, honeycomb, and traditional balsa construction.

6.1.1 Process Selection

Prior to the construction of the final aircraft, BoilerBus1 was built, flown, and crashed. BoilerBus1 was built as a prototype, and as such, was not built using the lightest construction techniques possible. The materials used were locally available or on-hand, inexpensive, and crash resistant. The fuselage was built using 1/8” plywood, to which the other components of the airframe were bolted. The wings were built around a balsa and spruce main spar, with balsa/fiberglass laminate leading edge to form a strong “D-tube” structure. Balsa wing ribs and built-up ailerons completed the wing structure, and the open portion of the wing, aft of the main spar, was covered in MonoKote iron-on covering. Tail surfaces were hot-wire cut EPS foam with carbon strip reinforcement for rigidity. The nose and tail fairings were hand shaped from insulation foam, and the landing gear were made from aluminum stock. The construction techniques introduced team members to basic model airplane construction methods and determined what techniques worked well for a given purpose. Through flight testing, the durability of the “D-tube” leading edge was verified, as the aircraft stalled on takeoff and struck the ground with its left wing tip, sustaining no damage. While the techniques and materials used resulted in a successful prototype airframe, they were much too heavy to be competitive.

In addition to the construction of the prototype aircraft, test wings and spars were built to be broken in order to verify the structural analysis. Successful teams in past years have used 1/32” balsa and 0.75 oz/yard fiberglass laminate to build entire airframes, so this method was investigated by vacuum bagging two separate simple wing structures. It was found that this method resulted in a very light and rigid wing structure and was thus implemented in the construction of the BoilerBus2 for the wing leading edge. Two spar designs were built to analyze the advantages and disadvantages of each. The balsa/carbon “O-beam” design was found to be very light and rigid in bending, while the all-balsa “I-Beam” was heavier, but better in torsion, as validated by the structural analysis.

In the end, the “O-beam” design was chosen to be used in the construction of the BoilerBus2 for its ability to resist bending along its length rather than torsion, as needed for the “D-tube” structure.

6.1.2 Component and Assembly Fabrication

The construction of the final airframe began with a CNC-cut wing mold of each wing half, as shown in Figure 6.1, in which the wing structure is assembled as a single piece. This was to ensure that the incidence of each wing-half was correct, and no twist was present along the span of the wing. The wings were assembled around a carbon fiber and balsa composite full-length main spar, to which a balsa and fiberglass laminate ‘D-tube’ leading edge was attached. Conventional balsa wing ribs formed the aft portion of the wing. The fuselage was then built around the wing spar structure, resulting in a one-piece airframe. The fuselage was comprised of a carbon fiber and balsa truss structure to support the weight of the payload and transfer the loads of the tail surfaces and motor. The carbon fiber/balsa sandwich landing gear were then attached directly to the main spar box and carbon fuselage stringers of the airframe. Tail surfaces were built using conventional model aircraft techniques, as they are proven, simple, and light. Figure 6.1 also shows the partially built aircraft using the techniques mentioned.

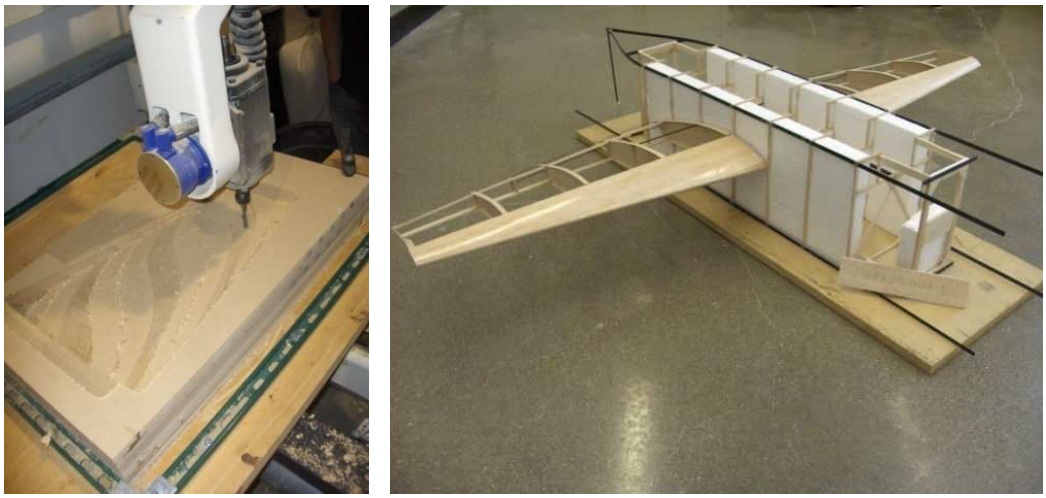

Figure 6.1: CNC Wing Mold and Construction of the Conventional Plane

6.2 Manufacturing Milestone Chart

The manufacturing milestone chart is illustrated in Figure 6.2. The planned schedule is shown in grey, while the actual timeline is given in gold.

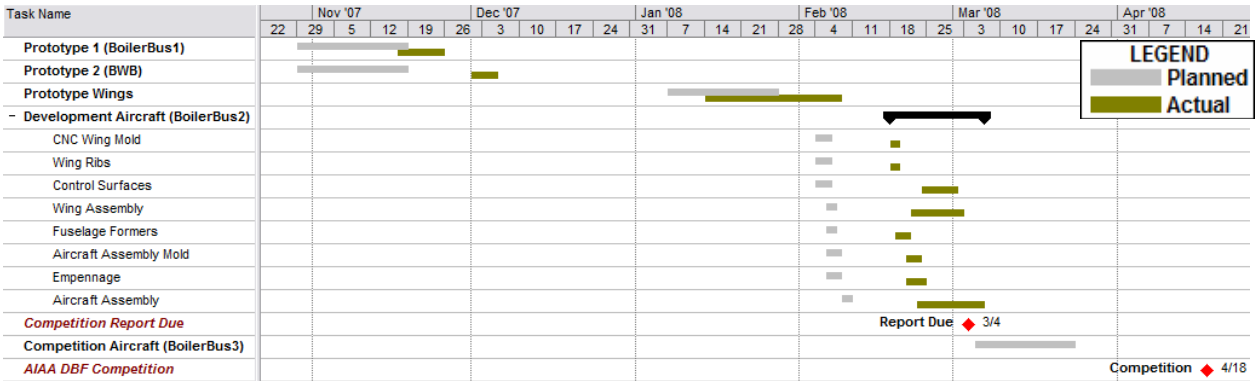

Figure 6.2: Manufacturing Milestone Chart

7 TESTING PLAN

Based on experiences learned in the first design spiral, testing was considered an integral part in verifying the design process. Four areas will be explored: structural, propulsion, ground mission, and flight testing. The objective will be to verify the structural integrity of the airframe & landing gear, the motor & propeller combination, deployment methods, and the flight model. The competition missions will be practiced by the pilot and ground crew for familiarity. The testing milestone chart is given in Figure 7.1, with the planned schedule in grey and the actual schedule in gold.

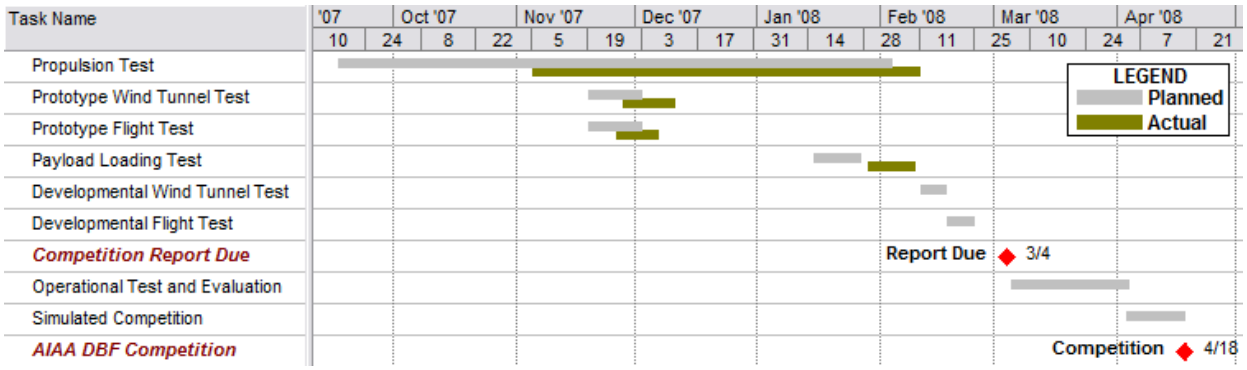

Figure 7.1: Testing Milestone Chart

7.1 Structural Testing

The aircraft will be loaded to max gross weight and the structural integrity of the aircraft will be confirmed by lifting the aircraft by its wingtips. This test will also be conducted at the competition as part of the technical inspection. The landing gear will be tested by means of drop tests from a fixed height. The height is determined by a maximum rate of descent value of 500 ft/min – a reasonable speed for a hard approach. This translates to a drop height of 13”. Several landing gear models will be constructed and each will be dropped with 11 lbs to simulate the hardest landing at max gross weight. The lightest gear that is able to withstand 10 simulated landings will be chosen. Ten was chosen as the number of simulations because the maximum possible number of landings at the competition is 5, allowing for a safety factor of two.

7.2 Propulsion Testing

The propulsion testing will consist of a static motor endurance test and dynamic motor tests for several propulsion configurations. The dynamic motor tests will simulate Mission 1 and Mission 2. Throughout each test, the wattage, voltage, current, and thrust will be recorded. The necessary equipment will be an Eagle Tree Watt Logger, a thrust stand, USB cables, a computer, and the propulsion system to be tested.

7.3 Payload Testing

Ground mission tests will involve testing the payload loading mechanisms, refining the payload compartment, and allowing the ground crew to practice for the competition. The payload restraint mechanisms will be refined to minimize the time required to actuate them, tailored to the ground crews' needs. During these ground tests the competition ground crew will be selected based on time trials.

7.4 Flight Testing

Flight testing will consist of three phases; control calibration, flight model confirmation, and competition mission analysis. The first phase: control calibration, will consist of several flights with minimal avionics onboard. The purpose of the flight will be to determine the actual handling qualities of the aircraft compared to predictions. In the flight model confirmation phase, an avionics package will be installed to record in-flight data to match the wind tunnel data. The lift-over-drag ratio will be found from making several glides at different trimmed speeds. The drag polar build-up will be accomplished by determining the L/D ratio. By combining these, the drag will be compared to that predicted by the wind tunnel. The final stage of flight testing will focus on mission analysis. In this stage of testing, each mission will be run through several times to determine the optimal takeoff and climb profiles, cruise speed, turn radii, and landing approaches. A flight testing checklist, as shown in Figure 7.2, is used to ensure that proper pre- and post-flight procedures are performed. Additionally, a consistent set of flight analysis questions are used to evaluate the flight tests according to the Cooper-Harper [14] pilot rating system.

Purdue University
AIAA DBF Flight Testing Card

Flight Test #	2
Mission Objectives:	Takeoff, complete two successful laps of course, develop feel for aircraft handling characteristics. Land on runway, without damage.

Batteries	
Secure	√
Voltage Before, V	15.4
Voltage After, V	13.7

Weather	
Temperature, F	44
Wind Velocity, mph	16
Wind Direction	SSW
Sky Conditions	clear

Pilot Feedback:
Aircraft rolled left on rotation, required right aileron input.
Aileron trim issues; possible servo centering problems?
Glides very well, enjoyable to fly
Landing uneventful, approach was long

Startup Procedure	
Transmitter ON	√
Receiver ON	√
Motor ON	√
Static Test	√

Shutdown Procedure	
Batteries OFF	√
Receiver OFF	√
Transmitter OFF	√
Battery Heat	moderate
Battery Voltage, V	13.7

Radio	
Range Check	√
Directional Check	√

Pilot Mission Objective Rating:	2

1, fully meets mission objectives
10, fails mission objectives

Figure 7.2: Flight Testing Checklist

8 PERFORMANCE RESULTS

8.1 Subsystem Performance

8.1.1 Propulsion

To supplement the computer analysis discussed in Section 5 with propeller performance characteristics, a series of wind tunnel tests were conducted on different propellers within the diameter range of 12" to 20". The experimental setup is shown in Figure 8.1. All of the propellers were tested on an AXI 4130 motor in Purdue's Boeing wind tunnel. The measurement system used consisted of the wind tunnel force balance (measuring thrust and drag), the Eagle Tree Data Logger (measuring RPM), and the Transducer Technologies torque sensor. Tests were conducted at different advance ratios, which is a function of forward velocity and propeller RPM. Experimental results were then used to evaluate the non-dimensional propeller parameters, namely advance ratio, coefficient of thrust, coefficient of power, and propeller efficiency.

Experimental results were then validated against Goldstein's theory [15], which gives an exact solution for propellers with finite blades operating under light loading. Goldstein's theory predicts propeller performance based on blade element theory, a bound vortex model (accounts for circulation distribution), and the vortex model (for induced velocity). In this approach, the propeller is stripped into a number of sections and at each section beta (zero lift line angle), chord, and airfoil characteristics are specified. Forces and power at each section are evaluated; total force and power are then obtained by integrating these sectional forces and power from root to tip. Figures 8.2 – 8.4 summarize the experimental and Goldstein's theory results for an 18" x 10" propeller. It can be observed from these figures that Goldstein's theory accurately predicts and validates the obtained experimental results. These results were then used to select the best motor-propeller combination for the given mission, which maximizes the overall score.

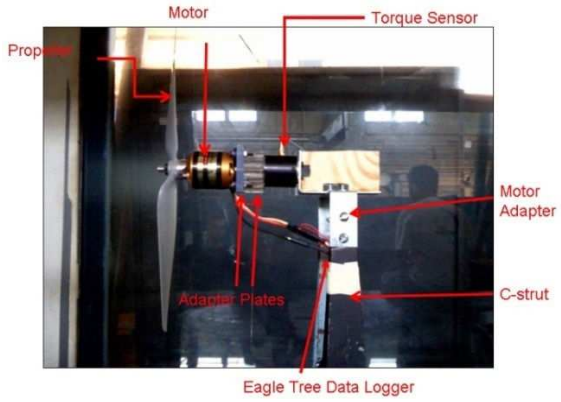

Figure 8.1: Experimental Setup

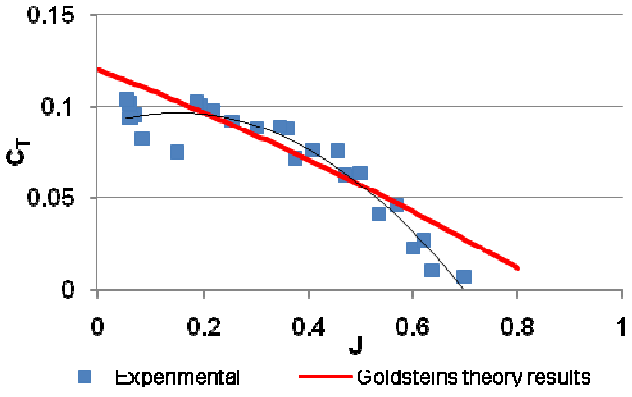

Figure 8.2: C_T vs. J for a 18" x 10" propeller

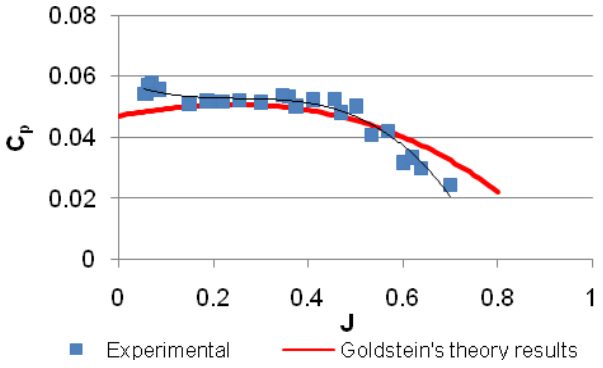

Figure 8.3: C_P vs. J for a 18" x 10" propeller

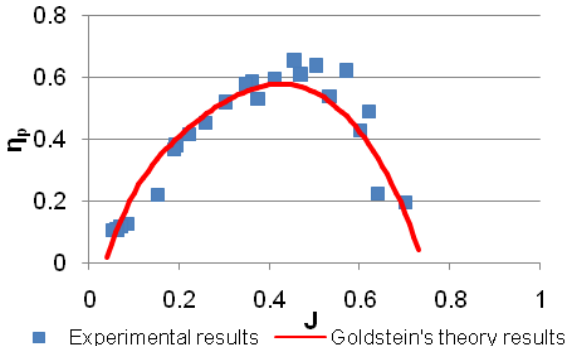

Figure 8.4: η_P vs. J for a 18" x 10" Propeller

8.1.2 Payload Configuration and Loading

Payload loading time for Mission 2 is a large part of the overall score, so the team held trials and practices to organize a ground crew to load the aircraft as quickly as possible. The set up was similar to what is expected at the competition. The ground crew started 10' behind the payload, which was separated 50' from a cardboard mock-up of the aircraft. The time required for the ground crew to pick up the required payload, load the aircraft, and return to the start line was recorded. Figure 8.5 compares the loading times for each payload combination.

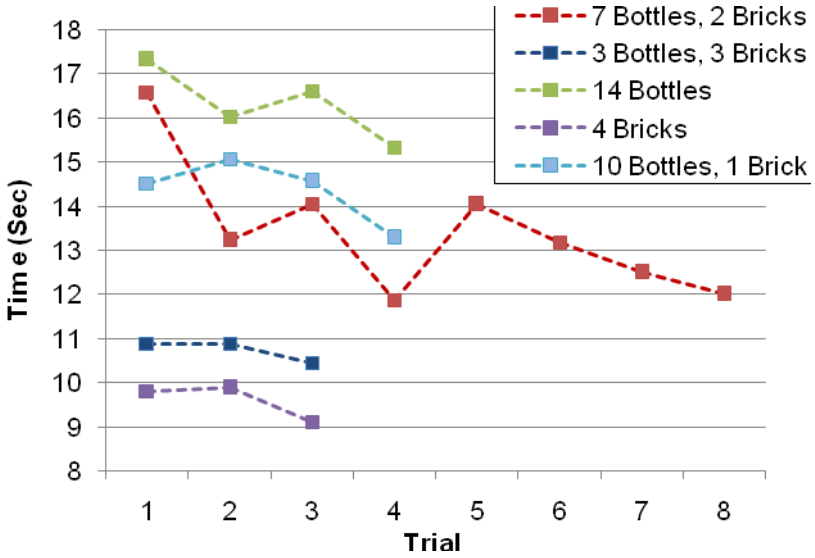

Figure 8.5: Loading Time Trials

The ground crew required more trials for combinations that were especially challenging, including ones which had more payload items to load in the aircraft. The downward trend in loading times shows that the ground crew was able to reduce loading time by perfecting loading techniques. The individuals on the ground crew developed specific roles, such as carrying the payload or opening restraint hatches. Contingency plans were developed in the event that the payloads are dropped on the way to the aircraft

or any other mishaps occur during loading. The ground crew was selected based on time trials and consists of three people plus one alternate.

8.2 Aircraft Performance

Performance predictions of the entire aircraft were validated using extensive wind tunnel and flight tests.

8.2.1 Wind Tunnel Testing

Wind tunnel testing was performed on both the BoilerBus1 and the BWB aircraft. Two main points were of interest: aircraft stability and aircraft aerodynamics. In order to accomplish both tests at once, the aircraft was mounted in the tunnel inverted with the supports mounted at the aircraft CG. The aircraft was balanced at the CG and allowed to pivot freely. This enabled the aircraft's pitch to be controlled by using the elevator. The BoilerBus1 mounted in the Boeing wind tunnel is shown in Figure 8.6.

Figure 8.6: Wind Tunnel Mount for Trimmed Drag Polar

Each aircraft was tested to ensure it was pitch-stable by confirming that the aircraft would return to trimmed flight once elevator input was released. Once the aircraft was found to be pitch-stable, the elevator was used to trim the aircraft over a range of C_L values from zero to stall. The trimmed drag polars and L/D versus flight speed for each of the aircraft are provided in Figures 8.7 and 8.8, respectively.

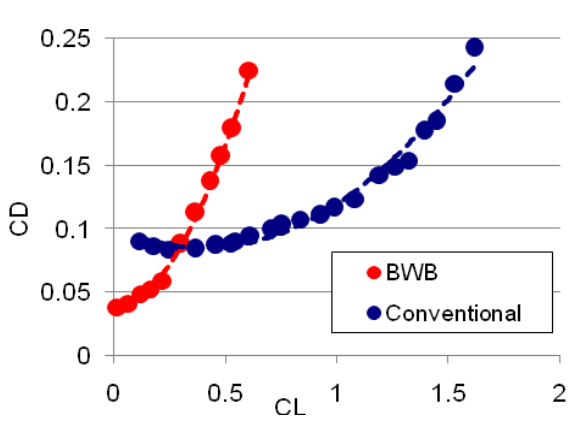

Figure 8.7: Trimmed Drag Polars

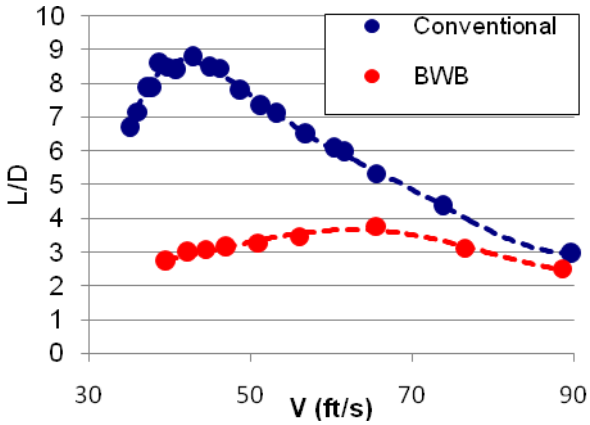

Figure 8.8: Lift to Drag Ratio

It is difficult to compare the two aircraft's drag polars due to the drastically different designs. However, the aircraft are designed to lift the same payload and thus it is easiest to compare the aircraft by the amount of lift and drag they produce with respect to dynamic pressure. From the drag polar, it can be seen that the conventional aircraft is capable of producing more lift than the BWB design, and the BoilerBus1 aircraft produced much less drag for a given amount of lift. The only advantage of the BWB design was a slightly lower C_{Do} value. However, most important to the score is minimizing battery weight, and thus the aircraft must have a high C_L value to minimize turn radius while also minimizing aerodynamic drag. For the cruise legs, it is very important to maximize L/D to maximize efficiency and minimize battery weight. The two aircraft were compared by using a fixed weight and determining the airspeed required to maintain level flight. The L/D ratio was then calculated. For the cases studied, the preliminary gross weight was used. The results are provided in Figure 8.8.

When the aircraft lift-to-drag ratios were compared, it was noted that the conventional aircraft had an L/D ratio 2.5 times larger than the BWB design. The maximum L/D ratio of the conventional design was found to be at 42 ft/s. This compares well to the initial prediction of 41 ft/s from the conceptual design.

In order to determine how the lift and drag predictions of the aircraft changed through the design process, the drag polars of the BoilerBus at several phases were plotted together, as seen in Figure 8.9. The first drag polar considered was the theoretical drag polar determined by the sizing analysis. This was then followed by CFD of the BoilerBus1 after all control surfaces were sized and the geometry was determined. Then wind tunnel testing was conducted on the aircraft, providing a third comparison. During detail design, CFD results for BoilerBus2 were obtained. The original theoretical model accurately predicted C_{Do} but slightly over-predicted drag due to lift, likely due to C_{Dmin} occurring at a non-zero angle of attack on the BoilerBus1. The CFD data accurately captured the trend of the lift to drag curve, but under-predicted C_{Do} due to the simplicity of the CAD model.

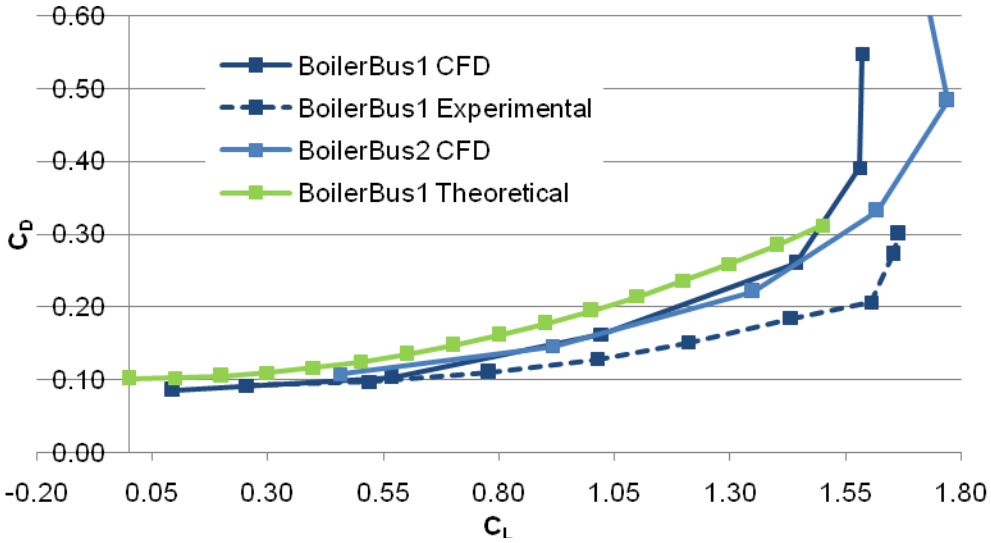

Figure 8.9: Drag Polar Comparison

8.2.2 Flight Testing

8.2.2.1 Validation

Preliminary flight testing was conducted on an existing pre-manufactured aircraft similar to the competition design requirements. The aircraft selected for the flight testing trials was a 1/5th scale Piper Cub. Its wing span was only 6" longer than what is allowed in the rules and its fuselage would not be able to fit the payloads, but its aspect ratio, wing loading, and total surface area were very close to that of the BoilerBus aircraft being considered for the competition. The motivation for these tests was to flight test an aircraft with known handling characteristics to determine what approaches yielded the most valuable flight test data and to establish a methodology for flight testing the prototype and final aircraft. The aircraft was equipped with the Eagle Tree Flight Data Recorder with an air data probe, GPS receiver, G-Force meter, and the Eagle Tree Power Logger to measure the motor power. Glide tests were performed to create the aircraft's drag polar. Constant power tests were performed at a range of different airspeeds to determine the power required at each airspeed. A turn analysis was conducted in an effort to determine which turning technique would require the least amount of energy: flat turns, wing-overs, or aerobatic maneuvers such as loops/ immelmens. Aerobatic maneuvers were found to be too risky to try with the aircraft during the competition. Level turns were found to be the optimal turning technique for both energy usage and safety.

8.2.2.2 Prototype Flight Testing

The BoilerBus1 prototype was flight tested shortly after its construction and pilot handling was assessed using the Cooper-Harper rating system, as shown in Figure 7.2. The aircraft completed three flights. The first two flights were performed at a weight of 9.5 lbs and were used for pilot familiarity of the aircraft and

for trimming the aircraft. The aircraft initially had trim issues due to asymmetry in the manufacturing of the wings. The glide tests of this flight were analyzed visually with video footage and indicated an approximate glide ratio in the range of 7:9, validating the predicted values from the wind tunnel tests and the CFD analysis. On the second flight, the aircraft had a slight cross wind and a pronounced yaw into the wind was produced resulting in a hard roll to the left. However, the roll was easily trimmed. The third flight was performed at the predicted max gross weight of 13 lbs. On takeoff, the plane rolled hard to the left, likely caused by a combination of the cross wind and torque from the motor. Due to the heavier weight, the wingtip stalled as a right roll was commanded, resulting in a wing strike and the termination of the flight. Minor damage resulted but the aircraft was easily repaired.

It was found that due to the short takeoff distance requirement, accurately being able to predict the distance was crucial to minimizing battery size and thus maximizing score. In order to verify the calculations, video footage of the BoilerBus1 test flight was used to calculate takeoff distance. The flight was done in calm winds, matching the conditions used in the propulsion analysis. Takeoff distance calculation was conducted by taking several image captures of the flight test video. Using the length of the aircraft (4') as a reference, the takeoff distance was able to be calculated, as seen in Figure 8.10. The aircraft systems, geometry, drag polar, and weight were then entered into to the propulsion analysis to determine the takeoff performance. The results can be seen in Table 8.10. Minimum and maximum values are included due to slight uncertainties on exactly when the aircraft is considered to have taken off. It can be seen that the takeoff analysis conservatively predicts takeoff distances.

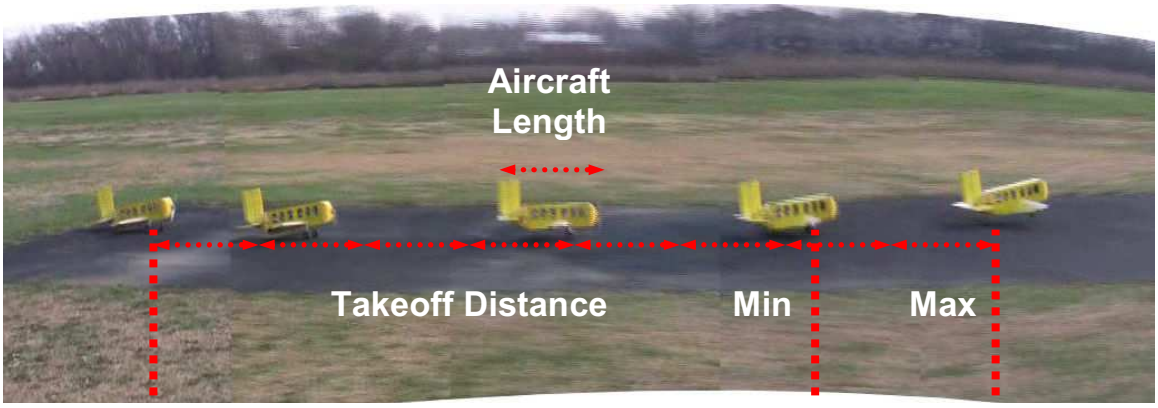

Figure 8.10: BoilerBus1 Takeoff Distance

Table 8.10: Takeoff Distances

	Analysis Takeoff Distance	Actual Takeoff Distance
Min	30'	25'
Max	32.5'	32'

9 REFERENCES

[1] Lowell, J A., "*Tree Diagrams*", URL: http://www.beager.com/~lifestar/qiwizard/tree.html, 1996

[2] Akao, Yoji [1994]. "Development History of Quality Function Deployment", The Customer Driven Approach to Quality Planning and Deployment. Minato-ku, Tokyo 107 Japan: Asian Productivity Organization, 339. ISBN 92-833-1121-3

[3] Cross, N., "Evaluating Alternatives," Engineering Design Methods, Wiley, New York, 1989, pp. 101-121

[4] Walkovitch, J., "The Joined Wing: An Overview," AIAA-85-0274, AIAA 23rd Aerospace Sciences Meeting, Reno, NV, Jan. 1985.

[5] Warren F. Phillips; A. B. Hansen; W. M. Nelson, "Effects of Tail Dihedral on Stability", *Journal of Aircraft*, 2006, 0021-8669 vol.43 no.6 (1829-1837)

[6] Brandt, Steven A., Stiles, Randall J., Bertin, John J., Whitford, Ray., "Introduction to Aeronautics: A Design Perspective" 2nd Edition, *AIAA Education Series,* AIAA, 2004.

[7] Raymer, D.P., *Aircraft Design: A Conceptual Approach*, 4th Ed., AIAA, Inc. Washington, DC. 2006.

[8] Smith, J., Batish P., Brandt S., and Morton S., "A student developed sizing methodology for electric powered aircraft applied to small UAVs," AIAA-2000-5536, 2000 World Aviation Conference, San Diego, CA, Oct. 2000.

[9] Roskam, Jan. Airplane Design, Part II: Preliminary Configuration Design and Integration of the Propulsion System, DARcorporation, Lawrence, KS, 1997.

[10] Roskam, Jan. Methods for Estimating and Control Derivatives of Conventional Subsonic Airplanes, 519 Boulder, Lawrence, KS, 1997.

[11] Lennon, Andy, *Basics of R/C Model Aircraft Design: Practical Techniques for Building Better Models*, Ridgefield, CT, 1996.

[12] Granta CES EduPack 2007, Purdue University

[13] UIUC Applied Aerodynamics Group, "UIUC Airfoil Coordinates Database - Version 2.0 (over 1550 airfoils)," University of Illinois at Urbana-Champaign, February 2008.[http://www.ae.uiuc.edu/m-selig/ads/coord_database.html. Accessed 8/1/08.]

[14] Cooper, G. E., and Harper, R. P., Jr., "The Use of Pilot Rating in the Evaluation of Aircraft Handling Qualities," NASA TN D-5153, April 1969.

[15] Sullivan, John P., "Advanced Theoretical Treatments of Propeller Aerodynamics*", Notes of Short Course presented at von Karmen Institute for Fluid Mechanics*, Brussels, Belgium, May 1982